



National University for Science and Technology  
POLITEHNICA BUCHAREST  
DOCTORAL SCHOOL OF AEROSPACE ENGINEERING

# PhD THESIS

**Study of the Mechanical Response of Ply-Level Hybrid Composites under Quasi-Static and Dynamic Loadings**

## SUMMARY

**PhD Student:** Ing. Maria DEMȘA (CASAPU)

**PhD Supervisors:** Prof. univ. dr. ing. Ion FUIOREA

Prof. univ. dr. ing. Michel ARRIGONI

**BUCUREȘTI**  
2023

## **KEYWORDS**

- carbon fiber
- composites
- hybridization
- Digital Image Correlation
- mechanical properties
- residual strain
- damage variable
- cyclic loading
- dynamic loading
- laser-induced shockwaves

## TABLE OF CONTENTS

INTRODUCTION .....	1
CHAPTER 1. STATE OF THE ART AND THEORETICAL BACKGROUND .....	3
INTRODUCTION.....	3
1.1 FIBER-REINFORCED COMPOSITE MATERIALS .....	3
1.1.1 Generalities .....	3
1.1.2 Fiber-reinforced hybrid composite materials.....	4
1.1.3 Failure Mechanism and Damage.....	4
1.2 QUASI-STATIC CONSTITUTIVE LAW AND DAMAGE FOR FIBER- REINFORCED COMPOSITES .....	5
1.2.1 Constitutive law.....	5
1.2.2 On-axis behavior and testing.....	6
1.2.3 Off-axis behavior and testing .....	7
1.2.4 In-plane shear properties.....	7
1.2.5 Damage assessment by cyclic load-unload off-axis test.....	7
1.2.6 Nonlinear constitutive model formulation.....	8
1.3 DYNAMIC LOADING OVERVIEW .....	10
1.3.1 Generalities .....	10
1.3.2 Experimental testing techniques for dynamic loading .....	11
1.3.3 Strain rate effects on fiber-reinforced composite materials .....	11
1.4 GENERALITIES ON LASER-INDUCED SHOCKWAVES .....	11
1.4.1 Principle and description of laser-induced shockwaves .....	11
1.4.2 Shockwave propagation.....	12
1.4.3 Tensile stress generation and velocity signal analysis for failure diagnosis...	13
1.4.4 Back-face velocity measurement techniques .....	14
1.4.5 Fiber-reinforced composites response under laser-induced shockwaves .....	15
SUMMARY .....	15
CHAPTER 2. TECHNICAL PERFORMANCES MEASUREMENTS OF THE MATERIALS .....	16
INTRODUCTION.....	16
2.1 MATERIALS AND LAMINATE CONFIGURATIONS .....	16

2.2	EXPERIMENTAL METHODS AND DATA ANALYSIS .....	17
2.2.1	Density measurements .....	17
2.2.2	Fiber weight fraction and fiber volume fraction .....	17
2.2.3	2D Microscopic Observations.....	17
2.2.4	Void content estimation .....	17
2.3	EXPERIMENTAL RESULTS AND DISCUSSION.....	17
2.3.1	Density measurements .....	17
2.3.2	Fiber weight and volume fraction .....	18
2.3.3	Microscopic observation.....	18
2.3.4	Void content estimation .....	20
	SUMMARY .....	21
	CHAPTER 3. QUASI-STATIC BEHAVIOR OF PLY-LEVEL HYBRID CARBON COMPOSITE MATERIAL.....	22
	INTRODUCTION.....	22
3.1	MATERIALS AND METHODS .....	22
3.1.1	Experimental setup .....	22
3.1.2	Sample description and preparation .....	23
3.1.3	Data processing .....	23
3.2	EXPERIMENTAL RESULTS AND DISCUSSION.....	24
3.2.1	On-axis tensile tests – 0° and 90° .....	24
3.2.2	Off-axis tensile tests .....	24
3.2.3	Damage assessment by Cyclic Load-Unload tensile tests .....	25
3.2.4	Predictions of off-axis nonlinear stress-strain response .....	25
	SUMMARY .....	26
	CHAPTER 4. DYNAMIC RESPONSE OF PLY-LEVEL HYBRID COMPOSITE MATERIALS .....	27
	INTRODUCTION.....	27
	PART 1: LASER-INDUCED SHOCKWAVES.....	27
4.1	SAMPLE DESCRIPTION.....	27
4.2	EXPERIMENTAL SETUP.....	28
4.3	LASER PULSE CHARACTERIZATION .....	28
4.3.1	Pulse Duration and Time Shift .....	28
4.3.2	Energy Measurements .....	29
4.3.3	Focal Spot Analysis .....	29
4.4	HETERODYNE VELOCIMETRY.....	29
4.4.1	Signal Processing .....	29
4.4.2	Speed of Sound Estimation from BFV Signals.....	29
4.4.3	Dynamic Tensile Strength and Strain Rate Estimation from BFV Signals by Novikov’s approach [82].....	30

Study of the mechanical response of ply-level hybrid composites under quasi-static and dynamic loadings

4.5	DAMAGE ANALYSIS PROCEDURE.....	30
4.6	REPEATABILITY OF EXPERIMENTS .....	31
4.7	EXPERIMENTAL RESULTS AND DISCUSSION.....	31
4.7.1	Along the fiber-direction (in-plane) laser-induced shockwave test results ....	31
4.7.2	Out-of-plane laser-induced shockwave test results .....	33
	PART 2: STEEL BALL IMPACT .....	35
4.8	SAMPLE DESCRIPTION AND EXPERIMENTAL SETUP.....	35
4.9	STEEL BALL IMPACT EXPERIMENTAL RESULTS .....	35
	SUMMARY .....	36
	CONCLUSIONS, CONTRIBUTIONS, AND OUTLOOKS .....	37
	CONCLUSIONS.....	37
	CONTRIBUTIONS.....	40
	OUTLOOKS .....	40
	PUBLICATIONS .....	41
	SELECTIVE BIBLIOGRAPHY .....	42

## INTRODUCTION

In the last decade, except during the pandemic lockdown, global air traffic has increased in power law [1]. In addition, air traffic is pointed out by its significant contribution to carbon emissions. To comply with ecological constraints and to supply air transport companies with the increasing demand for aircraft manufacturing, manufacturers are leading a commercial competition in which cost-effective solutions constrained with zero-fault reliability are key solutions. In this race, the use of composite materials in the aeronautic industry increased. As they are lightweight, they help decrease fuel consumption [2] and CO<sub>2</sub> emissions. Their mechanical properties are superior to traditional metals and can be tailored for a specific application [3]–[5]. Their remarkable strength-to-weight ratio, high specific modulus, and inherent corrosion resistance make them highly appealing for modern aircraft design.

As different fiber reinforcements have different mechanical properties, the most common attempt to improve or tailor the response of the composite to a specific load is by hybridization of the material, either intra-ply [6] or inter-ply [7], using two different types of fiber reinforcements. However, different fiber hybrid composites usually show a major load drop at the failure of the lower strain component, reducing the overall strength of the composite [8]–[10]. Consequently, this limitation restricts their application in high-added-value technologies. To address this challenge, alternative hybridization methods have been explored in recent years. Nonetheless, few studies are focused on the mechanical behavior of all-carbon fiber hybrid composites. After the development of thin-ply composites, which can enhance the mechanical and weight performance of the composites [11], compared to traditional thick-ply composites, another type of ply-level hybridization has been proposed consisting of mixing plies of different thicknesses in an attempt to obtain a targeted response of the material, without the use of other matrix or fiber reinforcements [12]. In light of these considerations, the integration of ply-level hybridization with all-carbon hybrid composites emerges as a promising avenue. This technique holds the potential to reduce manufacturing costs without compromising on superior technical performance.

The operational lifespan of aircraft exposes them to dynamic loadings, presenting a series of critical challenges. Jet engine blades and key aircraft components, notably the wing leading edge, face potential damage from foreign objects, such as bird strikes. These impacts can inflict significant harm on the aircraft's structural integrity. Moreover, a pressing concern involves containing a malfunctioning fan blade within the engine, safeguarding passengers and the airframe from harm. Achieving this dual objective requires the fan case structure to not only endure the impact but also maintain its structural stability during engine shutdown. Consequently, a comprehensive understanding of the dynamic behavior of materials used in the aerospace industry becomes imperative for designing structures that can withstand dynamic loads effectively.

As the aerospace industry has strong certification requirements and experimental tests can be quite expensive to perform for various load cases, it is necessary to use the ability of powerful computational methods to simulate the mechanical behavior of composites at the appropriate scale. These models provide an in-depth understanding of material deformation and failure that can be used to rethink the design approach in order to create stronger and safer structures and

enhance maintenance under operational conditions. However, in order to model the response of the structure subjected to dynamic loading, a specific mechanical model including constitutive law, equation of state, and damage model for the studied composite material is mandatory. The laser-induced shockwaves test can be an appropriate method for obtaining relevant data for material characterization at high strain rate loading, as well as information regarding the delamination threshold of the material subjected to dynamic loading in order to validate numerical models [13].

In this context, the primary aim of this thesis is to assess the impact of hybridization involving variations in both carbon fiber type and ply thickness. Specifically, this study introduces an all-carbon ply-level hybridization approach to investigate how it influences the internal structure, mechanical properties, and dynamic responses of unidirectional carbon fiber composites. To achieve this, a comprehensive material characterization is conducted, encompassing both quasi-static and dynamic loading conditions.

Aligned with the main objective of this thesis, the subsequent research goals were established:

- O1** – Experimental characterization of internal structure and physical properties of reference and ply-level hybrid unidirectional carbon composite materials
- O2** – Evaluate the quasi-static mechanical response of hybrid and reference laminates under on and off-axis tensile testing
- O3** – Investigate the cause of the nonlinear off-axis response through off-axis cyclic load-unload tensile tests and evaluate residual strains and damage variables
- O4** – Define a coupled damage-plasticity model to predict the nonlinear off-axis response of laminates
- O5** – Evaluate the shockwave propagation in the reference and ply-level hybrid materials, in the fiber direction and perpendicular to the fiber direction
- O6** – Induce delamination at high-strain rates and evaluate the dynamic tensile strength
- O7** – Evaluate the differences in damage position and threshold for the different configurations of the studied composites

Besides evaluating the effects of hybridization, these objectives also follow a fundamental characterization of unidirectional composites. This enables the incorporation of these materials into complex structures, providing a more robust understanding of their mechanical response and enhancing their potential across various applications.

The structure of the thesis is designed to organize the major experimental campaigns based on their complexity and strain rate category. The initial chapter offers a literature review covering topics such as fiber-reinforced composites, mechanical behavior under quasi-static and dynamic loading, and the theoretical foundation necessary to support the analysis conducted within this study.

Moving forward, the second chapter focuses on the materials employed in the research, the hybridization approach pursued, and the comprehensive characterization of physical properties like density and fiber volume content. Additionally, microscopic examinations of the internal structure are conducted, along with the identification of potential internal defects like voids and resin-rich regions.

The third chapter encompasses the complete range of experimental analyses carried out within the quasi-static regime. This involves studying both on and off-axis mechanical behavior, as well as assessing damage through cyclic load-unload testing and predicting nonlinear off-axis behavior. While the third chapter is dedicated to quasi-static testing, the fourth and final chapter contains the findings related to dynamic loading under high strain rates.

Detailed explanations of the testing setup and data processing for the laser-induced shockwaves technique are provided in the fourth chapter, along with the results obtained from impacts in both the fiber direction and perpendicular to it. The chapter also explores the setup and experimental findings of a steel ball impact test, which serves as a foundational step for future structural analyses.

## CHAPTER 1. STATE OF THE ART AND THEORETICAL BACKGROUND

### INTRODUCTION

This chapter provides the essential theoretical foundation for this thesis and discusses key research papers that are relevant to the subject. In accordance with the scientific approach followed in this work, first, the fiber-reinforced composite materials are reviewed, with an accent on the fiber-reinforced hybrid materials. The subsequent discussion encompasses the failure mechanisms inherent in fiber-reinforced composites, outlining the damages brought about by both low and high-velocity impacts.

Next, attention is directed towards describing the quasi-static response of unidirectional fiber-reinforced composites. This also involves a description of the theoretical formulations, testing protocols, and procedures for evaluating acquired data. Additionally, a comprehensive overview is provided concerning dynamic loading, centering on the fundamental principles of laser-induced shock wave theory.

### 1.1 FIBER-REINFORCED COMPOSITE MATERIALS

#### 1.1.1 Generalities

A structural composite refers to a material system characterized by two or more phases at a macroscopic level. The purpose of such a system is to achieve mechanical performance and properties that surpass those of the individual constituent materials in isolation. Typically, one of these phases is discrete, exhibiting greater stiffness and strength – often referred to as the reinforcement phase. Meanwhile, the other phase, known as the matrix, remains continuous, featuring lesser stiffness and strength.

Fiber-reinforced composites can use different types of fibers as reinforcement (glass, carbon, aramid, ceramic fibers), while the matrix is usually comprised of thermoset polymers or thermoplastics.

*Carbon fibers* are widely used for advanced composites and come in many forms with a range of stiffnesses and strengths depending on the manufacturing process [5]. Carbon fibers are well-known for being strong yet lightweight, they have high tensile strength, high chemical resistance, high stiffness, low thermal expansion, and low weight properties. Their mechanical properties are superior compared to glass fibers [14] which is why carbon fiber composites gradually replaced glass fiber composites in the aerospace industry [2].

For the matrix component of fiber-reinforced composites, thermoset polymers and thermoplastics are commonly used, but among the two, the most predominant types are thermoset polymers. The most commonly used thermosets are unsaturated polyesters, epoxies, polyimides, and vinylesters [5].

Advanced composite structures are usually in the form of unidirectional plies laminated together at various orientations, but they can also be used in the form of woven fabrics or textiles [5]. Prepregs, consisting of reinforcement fibers pre-impregnated with a precisely controlled amount of resin, offer superior uniformity and quality, ensuring consistent resin distribution and fiber impregnation [15]. Autoclave processing involves the curing of prepreg layups under

elevated temperature and pressure conditions. This process facilitates resin consolidation, ensuring minimal void content and enhanced mechanical properties. The combination of prepregs and autoclave processing results in aerospace components with exceptional strength-to-weight ratios, thermal stability, and performance consistency, critical for aircraft and spacecraft applications [16].

### **1.1.2 Fiber-reinforced hybrid composite materials**

Although carbon fiber composites exhibit superior mechanical properties compared to traditional metals and other types of fibers [3], they have low failure strain and exhibit a brittle behavior [17]. Hybridization with other types of fibers, either intra-ply or inter-ply, [6], [7], [18]–[20], or with metallic components [21], [22] has been studied as a method of increasing the damage tolerance and mechanical properties of carbon-fiber-reinforced composites.

After the development of thin-ply composites, which can enhance the mechanical and weight performance of the composites [11], compared to traditional thick-ply composites, another type of hybridization has been proposed – ply-level hybridization – consisting of mixing plies of different thicknesses in an attempt to obtain a targeted response of the material, without the use of other matrix or fiber reinforcements [12].

While an extensive number of research papers address the effects of glass-carbon fiber hybridization on the mechanical response of the composite laminate, few studies reported the mechanical behavior of all-carbon fiber hybrid composites. Curtis and Browne et al. [23] mixed the standard quality carbon fiber plies in the principal load direction of a quasi-isotropic laminate with ultra-high performance carbon fibers, Naito et al. [24] combined high strength with high modulus carbon fibers and performed  $0^\circ$  quasi-static tensile testing, Czel et al. [25] used an all-carbon hybridization approach to obtain a pseudo-ductile failure response of the unidirectional carbon fiber composites by blocking low strain to failure, high and ultra-high modulus carbon fibers with outer layers of high strain to failure and intermediate modulus carbon fibers.

While these studies presented the effects of the hybridization of different types of carbon fiber with similar ply thickness, another type of all-carbon hybridization approach has been proposed by Furtado et al. [26]. To improve the notched response of thin-ply composites they introduced the concept of ply-level hybridization which consists of mixing in the same laminate prepregs with different ply thicknesses, without changing the fiber and matrix system. The effect of such a hybridization on the unnotched and notched response of quasi-isotropic laminates was studied and their work revealed that when using a selective hybridization, no significant difference was observed in the unnotched tensile strength.

### **1.1.3 Failure Mechanism and Damage**

#### *1.1.3.1 Failure Mechanism*

When a laminate undergoes various types of loading, whether in-plane or through-thickness, it is susceptible to the initiation and propagation of damage. This can ultimately lead to the failure of the composite structure. Common types of damage include fiber fracture, matrix cracking, fiber-matrix separation, and delamination.

The failure of composites does not happen abruptly. Typically, fracture mechanisms evolve hierarchically. Although their rate of propagation and mutual influence may be influenced by the microstructure, the sequence and location of their occurrence remain relatively consistent across various materials and loading conditions. The first step represents the decohesion between the fiber and the matrix. It occurs as microcracks appear in the matrix at the scale of the fiber, mainly due to manufacturing residual stresses.

The second step is represented by the propagation of the matrix crack. During the loading phase, the diffuse damage continues to propagate and develop into transverse and shear stresses. As loading intensifies, the damage propagates, resulting in transverse cracking in the ply perpendicular to the loading direction.

The third step is represented by local delamination. Because of the stress concentration at the transverse crack tip, local delamination occurs at the interface between plies. The fourth step is represented by the fiber rupture. As the delamination prevents the transmission of the loads between the plies, the load will only be supported by part of the fibers, leading to their overload and fiber rupture. The final stage is represented by the entire failure of the material.

### 1.1.3.2 Impact damage

When subjected to impact loading, depending on the impact energy level, the impact damage in composite materials can be divided into three categories:

- Barely Visible Impact Damage (BVID) – this type of damage can occur under low-velocity and low-energy impact (1 to 5 J [27]) leading to an invisible impact damage underneath the surface of the laminate, such as a delamination between adjacent layers inside the material, which is difficult to detect visually [28].
- Visible Impact Damage (VID): With the increase of the impact energy, clear dents will occur on the laminate surface around the impact zone. In addition, the large internal delamination area or matrix cracking can be observed by C-scan or other scanning methods, or simply visible on semi-transparent composite materials.
- Perforation damage: It usually occurs when the laminate is subjected to high-velocity impact and the energy level is large enough to perforate the laminate, which often leads to complete failure of the material in the impact area, engendering a plume of debris.

Composite materials have several failure modes, and the strain rate sensitivity can result in a change from one failure mode to the other. The impact damage mechanism in a laminate is a very complex process as it represents a combination of matrix cracking, surface buckling, delamination, fiber shear-out, fiber fracture, etc., which usually all interact with each other [29].

Under low-velocity out-of-plane impact, the initial form of damage that emerges is matrix cracking in the transverse direction, followed by delamination if the loading persists.

For high-velocity and ballistic impact, the structure has less time to respond and therefore, the damage does not propagate as in the case of low-velocity impact. The architecture of the reinforcement can influence the energy absorption mechanism and also, for different materials such as carbon, glass, or Kevlar, different mechanisms can dominate [27], [30], [31].

## 1.2 QUASI-STATIC CONSTITUTIVE LAW AND DAMAGE FOR FIBER-REINFORCED COMPOSITES

### 1.2.1 Constitutive law

The unidirectional ply is a widely form of the elementary component of the fiber-reinforced composite laminates. Its cured mechanical characteristics are orthotropic, with higher mechanical performance in the longitudinal direction, also called fiber direction – designated as 1, than in the two other orthogonal directions, called transverse directions – designated as 2 and 3. The elastic behavior of an orthotropic material is characterized by 9 elastic constants, and the constitutive equations (compliance matrix) for orthotropic materials, in terms of engineering constants, can be written in the form of equation (1.1) [27].

$$\begin{bmatrix} \varepsilon_{11} \\ \varepsilon_{22} \\ \varepsilon_{33} \\ \gamma_{23} \\ \gamma_{13} \\ \gamma_{12} \end{bmatrix} = \begin{bmatrix} \frac{1}{E_{11}} & -\frac{\nu_{21}}{E_{22}} & -\frac{\nu_{31}}{E_{33}} & 0 & 0 & 0 \\ -\frac{\nu_{12}}{E_{11}} & \frac{1}{E_{22}} & -\frac{\nu_{32}}{E_{33}} & 0 & 0 & 0 \\ -\frac{\nu_{13}}{E_{11}} & -\frac{\nu_{23}}{E_{22}} & \frac{1}{E_{33}} & 0 & 0 & 0 \\ 0 & 0 & 0 & \frac{1}{G_{23}} & 0 & 0 \\ 0 & 0 & 0 & 0 & \frac{1}{G_{13}} & 0 \\ 0 & 0 & 0 & 0 & 0 & \frac{1}{G_{12}} \end{bmatrix} \begin{bmatrix} \sigma_{11} \\ \sigma_{22} \\ \sigma_{33} \\ \tau_{23} \\ \tau_{13} \\ \tau_{12} \end{bmatrix} \quad (1.1)$$

### 1.2.2 On-axis behavior and testing

Quasi-static tension tests along  $0^\circ$  and  $90^\circ$  fiber orientations are performed with the use of electro-mechanical or hydraulic testing equipment, to determine the tensile properties in the longitudinal and transverse directions of the unidirectional laminates.

Longitudinal properties associated with loading in the fiber direction are dominated by the fibers, which are usually stronger, stiffer, and have a lower ultimate strain than the matrix [5]. To analyze the behavior of composite materials under tensile or compressive loading and compare the results with other studies, standard procedures must be followed. “ASTM D3039/D3039M - Standard Test Method for Tensile Properties of Polymer Matrix Composite Materials” [32] can be used for tensile loading as well as BS EN ISO 527-5:2009: Plastics. Determination of tensile properties. Test conditions for unidirectional fibre-reinforced plastic composites [33].

In the transverse to the fiber direction, the behavior of unidirectional composites, especially the strength, is dominated by the matrix and interfacial properties. Under tensile loading, the behavior of unidirectional composite materials is quasi-linear, with relatively low ultimate strengths and strains [5].

In the case of failure stress in the fiber direction, thickness and size effects due to the geometry of the tested sample were reported in the literature. [34], [35]. Kawai et al. [35] proposed a geometrical scaling for the failure stress of the  $0^\circ$  tensile test specimens. Using equation (1.2), where  $\sigma_{ref}$  – failure stress of laminate with reference thickness,  $t_{ref}$  – reference laminate thickness,  $\sigma$  – calculated failure stress,  $t$  – laminate’s thickness for which failure stress is calculated,  $m$  – fitting exponent, a 1D thickness scaling can be performed. If another dimension of the sample varies, such as the width, a 2D geometrical scaling can be performed. In this second scaling, the reference failure stress of laminate (with reference thickness)  $\sigma_{ref}$  is scaled based on the gauge area (length  $\times$  width) of the new-dimension laminate  $A$  and the gauge area of reference laminate  $A_{UTS13}$ , using equation (1.3), where  $n_2$  represents a fitting exponent. The exponent  $m$  from equation (1.2) is also scaled using equation (1.4), based on the initial exponent determined from the reference laminates  $m_{UTS}$ .

$$\frac{\sigma}{\sigma_{ref}} = \left( \frac{t}{t_{ref}} \right)^{-\frac{1}{m}} \quad (1.2)$$

$$\sigma_{ref} = \sigma_{UTS13} \left( \frac{A}{A_{UTS13}} \right)^{n_2} \quad (1.3)$$

$$-\frac{1}{m} = -\frac{1}{m_{UTS}} \left( \frac{A}{A_{UTS13}} \right)^{n_1} \quad (1.4)$$

### 1.2.3 Off-axis behavior and testing

To characterize the behavior of unidirectional composites, the off-axis tensile test has received much attention as it can be used to verify the applicability of tensor transformation equations for the elastic properties of the fiber composite [3], [36]. The off-axis tensile test also serves as a convenient method for estimating the in-plane shear properties, eliminating the need for specialized fixtures or composite samples designed specifically for this purpose [37]–[40]. Furthermore, the off-axis test can be employed to evaluate the strength properties of the composite in various in-plane loading directions. This capability is valuable for design and optimization purposes, enabling a comprehensive understanding of the material's behavior and facilitating informed decision-making.

From a macro-mechanical point of view, the off-axis mechanical properties of unidirectional fiber-reinforced composites are anisotropic due to variations in fiber orientation with respect to the loading axis.

If the composite is transversely isotropic and the in-plane elastic properties are known ( $E_1$  – elastic modulus in the fiber direction,  $E_2$  – elastic modulus in the transverse direction,  $\nu_{12}$  – major Poisson ratio,  $G_{12}$  – in-plane shear modulus), the off-axis apparent elastic modulus  $E_x$  can be predicted using the transformation equation (1.5) and the apparent Poisson ratio  $\nu_{xy}$  can be predicted by using equation (1.6), for any off-axis angle  $\theta$ .

$$\frac{1}{E_x} = \frac{1}{E_1} \cos^4 \theta + \left[ \frac{1}{G_{12}} - \frac{2\nu_{12}}{E_1} \right] \sin^2 \theta \cos^2 \theta + \frac{1}{E_2} \sin^4 \theta \quad (1.5)$$

$$\nu_{xy} = E_x \left[ \frac{\nu_{12}}{E_1} (\sin^4 \theta + \cos^4 \theta) - \left( \frac{1}{E_1} + \frac{1}{E_2} - \frac{1}{G_{12}} \right) \sin^2 \theta \cos^2 \theta \right] \quad (1.6)$$

### 1.2.4 In-plane shear properties

The behavior of a unidirectional composite under in-plane shear loading is dominated by the matrix properties and the local stress distributions [5]. The shear behavior of unidirectional composite laminates can be decomposed into two parts, a linear behavior and a second nonlinear behavior followed by the rupture of the material, as was reported by several authors [41]–[44].

Various experimental approaches can be used to characterize the shear behavior of unidirectional composite materials, each having advantages and disadvantages, as a state of pure shear is difficult to obtain experimentally.

Despite lacking standardization, the off-axis tensile test has received significant interest as a means of establishing a straightforward method for characterizing the shear properties of composite materials. Pindera et al. [37] conducted a study on seven off-axis configurations 5°, 10°, 15°, 30°, 45°, 60°, and 75°. They noted that the 45° specimen is an excellent specimen for accurate determination of  $G_{12}$ , as the error due to shear stress vanishes in calculating  $G_{12}$ .

When the shear strength cannot be accurately evaluated experimentally, to obtain an approximate shear strength, the Tsai-Hill failure criterion for uniaxial off-axis strength [36] represents an alternative. The Tsai-Hill failure criterion is detailed in equation (1.7), in which  $\theta$  is the off-axis angle,  $X$  is the failure stress in the fiber direction,  $Y$  is the failure stress in the direction perpendicular to the fiber and  $S$  represents the shear failure stress or shear strength. The shear strength  $S$  is adjusted so that the failure stress prediction using the Tsai-Hill criterion fits the off-axis experimental data for failure stress.

$$\frac{\cos^4 \theta}{X^2} + \left[ \frac{1}{S^2} - \frac{1}{X^2} \right] \cos^2 \theta \sin^2 \theta + \frac{\sin^4 \theta}{Y^2} = \frac{1}{\sigma_{xx}^2} \quad (1.7)$$

### 1.2.5 Damage assessment by cyclic load-unload off-axis test

Different models used to predict the nonlinear behavior of unidirectional fiber-reinforced composites loaded off-axis attribute the nonlinearity of the response either to plastic

deformation of the matrix [45]–[48], to internal damage and stiffness reduction [49], [50] or both [51]–[56].

To investigate the cause for nonlinear behavior in off-axis tests for the composite materials, cyclic load-unload tests can be performed, with the amplitude of the stress level increasing for each cycle. This approach has been proposed by Ladeveze and Le Dantec [56] and they associated the stiffness reduction with a damage variable, based on continuum damage mechanics, while a plasticity model takes into account the residual strains with complete unloading. The damage variable can be calculated from the cyclic load-unload tests using equation (1.8), where  $E_i$  represents the modulus of the  $i^{\text{th}}$  cycle and  $E_0$  represents the initial elastic modulus of the first cycle. The residual strain (or plastic strain), needed for identifying the parameters for a plasticity model, can be extracted as well from the cyclic load-unload modulus using relation (1.9) where  $\sigma_i$  is the maximum stress in the  $i^{\text{th}}$  cycle, which should be as close as possible to the maximum stress levels imposed in the test setup.

$$D = 1 - \frac{E_i}{E_0} \quad (1.8)$$

$$\varepsilon_{res} = \varepsilon_i - \frac{\sigma_i}{E_i} \quad (1.9)$$

In Ladeveze's work, the elastic modulus of the cycle  $E_i$  is evaluated as the unloading chord modulus from the endpoints of the loading and unloading part of the  $i^{\text{th}}$  cycle, as shown in Fig. 1.1a, such that the effects of the load-unload hysteresis are minimized [55].

While Ladeveze's approach is widely used in the literature, two other proposals for the evaluation of the elastic modulus of the cycle were found, which are less researched. Fitoussi et al. [57] and Hug [58] suggested taking the cycle modulus as the slope of a linear regression of the loading curve of the cycle, taken between  $\sigma_{xi}/10$  and  $\sigma_{xi}/2$ . An illustration of this method is found in Fig. 1.1b. Castres [59] suggested another approach, by applying a successive linear regression on the loading curve of each cycle and selecting the modulus as the slope of the linear regression that has a maximum coefficient of determination  $R^2$ , denoted as the Regression method.

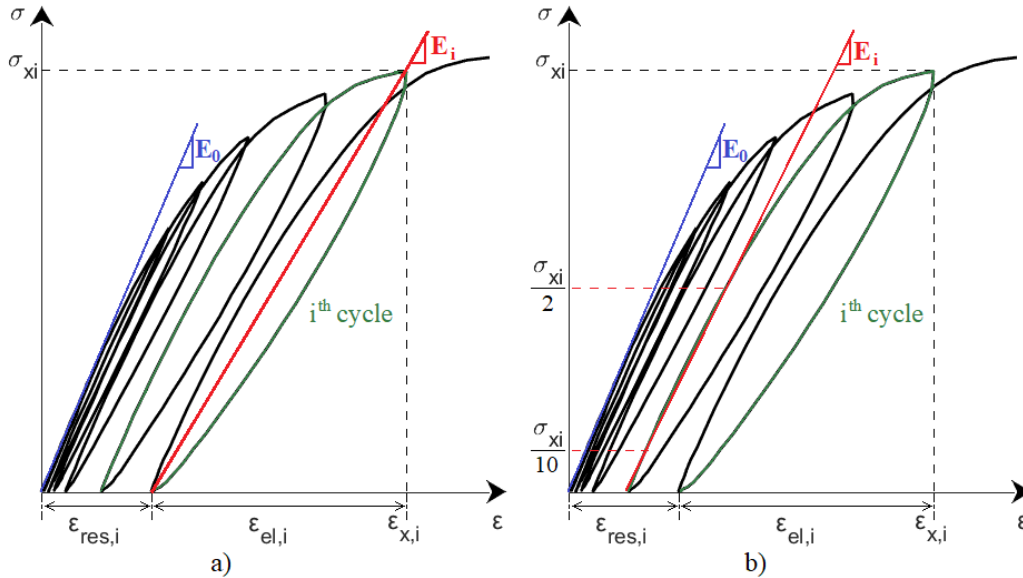


Fig. 1.1. Methods of determination of damage variable  $D$  and residual strain  $\varepsilon_{res}$  from load-unload cycles; a) Ladeveze's method, b) Fitoussi's method

### 1.2.6 Nonlinear constitutive model formulation

A coupled damage-plasticity model similar to the one proposed by Zhai et al.[60] can be defined, to model and predict the off-axis nonlinear behavior of unidirectional composite materials. In the model, the nonlinear off-axis behavior exhibited by the unidirectional fiber

composites is attributed to both damage and plasticity. The damage is characterized by stiffness loss with each load-unload cycle, and plasticity is defined by the residual strains with complete unloading.

To account for the influence of both parameters, the incremental strain is decomposed into elastic and plastic strain increments, as proposed by Sun et al [45]. Equation (1.10) shows the components of the incremental strain, where  $\varepsilon_x$  represents the macroscopic axial strain,  $\varepsilon_x^e$  is the elastic strain, and  $\varepsilon_x^p$  is the plastic strain component.

$$d\varepsilon_x = d\varepsilon_x^e + d\varepsilon_x^p \quad (1.10)$$

### 1.2.6.1 Plastic strain formulation

By using an associated flow rule, the incremental plastic strain can be written in terms of the stress  $\sigma_{ij}$  ( $i, j = 1, 2, 3$ ) in the principal material directions, the plastic potential function  $f$  and a scalar function of proportionality  $\lambda$ , as shown in equation (1.11) [45], [46], [61].

$$d\varepsilon_x^p = \frac{\partial f}{\partial \sigma_{ij}} d\lambda \quad (1.11)$$

Cho's [46] plastic potential function formulation is employed in this study. The plastic potential function is defined as shown in equation (1.12), where  $\sigma_{ij}$  ( $i, j = 1, 2$ ) are the stresses in the material principal directions,  $a_2$ , represents a plastic anisotropy parameter, and  $b_2$  also represents a plastic anisotropy parameter, for the dilatational component of the plastic potential function.

$$f = \sqrt{a_2 \sigma_{22}^2 + \sigma_{12}^2} + b_2 \sigma_{22} \quad (1.12)$$

The effective stress  $\bar{\sigma}$  is defined as being equal to the plastic potential function  $f$ , and the proportionality factor is derived from the increment of plastic work per unit volume  $dW^p$ , and the scalar function of proportionality is derived as equal to the incremental effective plastic strain.

Sun and Chen [45] proposed using a power-law function to fit the master effective stress–effective plastic strain curve. Thus, the effective plastic strain can be expressed as shown in equation (1.13), where the coefficients  $A$  and  $n$  are to be determined from experimental data.

$$\bar{\varepsilon}_p = A(\bar{\sigma})^n \quad (1.13)$$

The effective stress can be expressed in terms of off-axis angle and applied stress as:

$$\bar{\sigma} = h(\theta)\sigma_x \quad (1.14)$$

where

$$h(\theta) = \sqrt{a_2 \sin^4 \theta + \sin^2 \theta \cos^2 \theta} + b_2 \sin^2 \theta \quad (1.15)$$

Moreover, the effective plastic strain increment  $d\bar{\varepsilon}_p$  can be derived from the measured plastic strain increment  $d\varepsilon_x^p$  as:

$$d\bar{\varepsilon}_p = \frac{d\varepsilon_x^p}{h(\theta)} \quad (1.16)$$

For proportional loading, equation (1.16) can be integrated into [46]:

$$\bar{\varepsilon}_p = \frac{\varepsilon_x^p}{h(\theta)} \quad (1.17)$$

For each load-unload cycle, the effective plastic strain and effective stress can be calculated from the experimental axial stress and axial plastic strain, also referred to as residual strain. Regardless of the off-axis angle, the curve  $\bar{\sigma} - \bar{\varepsilon}_p$  should be almost the same [45]. Therefore, by trial and error,  $a_2$  and  $b_2$  are tuned so that  $\bar{\sigma} - \bar{\varepsilon}_p$  curves from different off-axis tests are as

Study of the mechanical response of ply-level hybrid composites under quasi-static and dynamic loadings coincident as possible. After  $a_2$  and  $b_2$  are determined, the curve  $\bar{\sigma} - \bar{\varepsilon}_p$  is fitted with the power function in equation (1.13), and  $A$  and  $n$  parameters are extracted.

### 1.2.6.2 Elastic strain formulation and nonlinear coupled damage-plasticity constitutive model

Using the formulation of the damage variable in equation (1.8), the elastic strain increment from equation (1.10) can be written as

$$d\varepsilon_x^e = \frac{d\sigma_x}{(1-D)E_0} \quad (1.18)$$

where  $D$  represents the damage variable,  $E_0$  is the initial elastic modulus of the undamaged material, and  $\sigma_x$  is the applied axial stress.

To incorporate the damage variable  $D$  into a constitutive model, Xie et al. [61] proposed expressing the damage variable in terms of the effective stress, in the form of a Weibull distribution function, as shown in equation (1.19), where  $n_e$  and  $\sigma_e$  are parameters that can be determined by fitting the experimental data, and  $\bar{\sigma}$  represents the effective stress.

$$D = 1 - \exp\left(-\left(\frac{\bar{\sigma}}{\sigma_e}\right)^{n_e}\right) \quad (1.19)$$

The expression of the axial strain can be written in terms of the applied stress, the off-axis angles, and the parameters for the constitutive model as written in equation (1.20)

$$\varepsilon_x = \frac{\sigma_x}{E_x \cdot \exp\left(-\left(\frac{\sigma_x h(\theta)}{\sigma_e}\right)^{n_e}\right)} + A\sigma_x^n (h(\theta))^{n+1} \quad (1.20)$$

## 1.3 DYNAMIC LOADING OVERVIEW

### 1.3.1 Generalities

In general, the fluid-structure interaction and impact response of materials can be described by their physical modifications after being recovered (melting, deformation, cracks, ...). They are classified depending on the velocity of the projectile [27].

- **Low-velocity impacts** are considered to occur at velocities below 10 m/s;
- **Intermediate-velocity impacts**, which represent a transition regime between low and high-velocity impacts, are at velocities between 10 m/s and 50 m/s.
- **High-velocity impacts** range from 50 m/s up to 1000 m/s.
- **Hyper-velocity impact**, at velocities above 1000 m/s.

The material response depends on the stress intensity - and its duration - and also, the stress or strain rate. In low-velocity impact, the structure has more time to respond to the impactor and as a consequence, more impact energy can be absorbed by the structure which can also lead to extensive damage within the structure [31].

With the increase of the impact velocity of the projectile, the shock-induced stress increases, and thus the damage in the composite structure is more localized [62]. In high-velocity impact, the structure has less time to respond to the sudden load, as the response of the material is dominated by the stress-wave propagation through the target's thickness [31], therefore leading to a local deformation at the impact point, and often perforation of the structure [63]. Thus, understanding perforation mechanism and failure is important when studying materials intended to be used in applications where high-velocity impact represents a threat.

Ballistic impact is generally a low-mass high-velocity impact caused by a propelling source [30].

Impact energy is the maximum kinetic energy of the impactor at the time of impact into the sample. For impacts without perforation of the target, it also represents the energy introduced into the specimen [64].

### 1.3.2 Experimental testing techniques for dynamic loading

For low strain rates, below  $10 \text{ s}^{-1}$ , servohydraulic machines can be used. They are not suitable for higher strain rates because of the inertial effects of the heavy load cells and grip [65].

A brief description of another method to test composites at intermediate and high strain rates is given in [66]. The Hopkinson bar technique permits the determination of the variation of basic material properties as a function of strain rate. Several types of Hopkinson bars are currently employed; these include the punchloaded Hopkinson bar, the compression bar, the tensile bar, and the Hopkinson bar shear test. Strain rates approaching  $1000 \text{ s}^{-1}$  can then be achieved using gas-driven projectiles to accelerate the weighbar and, in turn, load the input bar.

Besides the Hopkinson bar technique, Hsiao et al. [65] used a drop tower for dynamic compressive testing of thick composites.

For high-velocity impact studies, the single-stage gas gun is generally used. The specimen is clamped between frames to be kept in position while being hit by the projectile. The projectile's velocity can be modified by varying the pressure of the gas in the firing chamber.

For very high strain rates and shockwave studies, plate-impact techniques can be used. With this technique, a metallic or polymeric flyer plate hits the tested target at an impact velocity ranging from a few tens of meters per second to a few thousand meters per second.

Another method of generating very high strain rate loadings is by using laser-induced shockwaves [67]. This technique was initially developed for studying bonded material adhesion. It was employed for composite material bonding assessment [68], delamination observation under out-of-plane high strain rate loading [69], [70], controlled delamination in carbon fiber composites [71], and delamination in UHMWPE composites [13].

### 1.3.3 Strain rate effects on fiber-reinforced composite materials

Numerous investigations have tackled the issue of composite material response under different strain rate conditions, revealing a noticeable impact of strain rate on the mechanical characteristics of these materials.

Harding and Welsh [72] showed that the influence of the strain rate is barely observed in tensile loading in the longitudinal direction of unidirectional carbon/epoxy composites.

For tensile loading in the transverse direction for unidirectional composites, strain rate sensitivity is more pronounced [73]. An increasing modulus and strength for increasing strain rates for unidirectional carbon/epoxy was reported by Gilat et al. [74] but he also reported no considerable effect on the failure strain, for strain rates between  $10^{-5} \text{ s}^{-1}$  and  $400 \text{ s}^{-1}$ .

For the transverse compressive behavior, Hsiao and Daniel [65] showed that transverse strength, which is a matrix-dominated property, shows nearly a two-fold increase from the quasi-static value.

## 1.4 GENERALITIES ON LASER-INDUCED SHOCKWAVES

### 1.4.1 Principle and description of laser-induced shockwaves

Laser-induced shockwaves have been used to induce a dynamic loading in materials since the first work of White in 1963 [75]. Later on, the possibility of measuring the free-surface velocity extended its application [76], [77]. Several studies addressed the dynamic loading and failure of metallic materials in the 90s [76]–[79] and also the adherence of thin film coatings [80].

Laser-induced shockwaves are produced when focusing a short-duration ( $\sim$ ns) and high-energy ( $\sim$  J) pulsed laser beam on a small solid surface. When focused on a material, the photonic energy is absorbed by condensed matter and as a consequence, the surface of the irradiated material is sublimated. The plasma resulting from the sublimation expands rapidly, which induces a shockwave into the target material, similar to a surface explosion effect. The maximal pressure of this shockwave is called the ablation pressure and depends on the laser source characteristics and the irradiated material. The shockwave then propagates through the

thickness toward the target's back face, according to the material properties. For these experiments, the concept of incident energy is less relevant than that of incident laser density of power (intensity), which takes into account not only the energy but also the laser irradiation time and the impacted surface. The density of power can be determined based on equation (1.21), where  $\phi$  is the density of power,  $E$  represents the laser beam energy,  $\tau$  is the pulse duration and  $S$  is the surface irradiated by the laser beam.

$$\phi \left( \frac{GW}{cm^2} \right) = \frac{E(J)}{\tau(ns) \cdot S(cm^2)} \quad (1.21)$$

The plasma expansion can be confined by adding a solid (glass) or liquid (water) transparent media to the laser irradiation on the irradiated surface, slowing down the plasma expansion. The coating layer, or sacrificial layer, is usually used between the target surface and the confining medium in order to absorb the plasma-induced thermal effects [71], and have a well-known laser matter interaction.

### 1.4.2 Shockwave propagation

In order to bring a simplified understanding of shock propagation, conservation laws in 1D geometry are applied to the case of the propagation of a shock wave, treated as a discontinuity. The parameters ahead of the shock front are pressure  $P_0$ , temperature  $T_0$  and density  $\rho_0$ , and material velocity  $u_0$  (assumed to be zero here). The corresponding parameters behind the shock front are  $P$ ,  $T$  and  $\rho$ . The front velocity is  $D$ , and behind it, the material velocity is  $u$ . The expressions for conservation of mass, momentum and energy across a shock front are also known as Rankine-Hugoniot relations.

$$\text{Mass conservation: } \rho_0 D = \rho(D - u) \quad (1.22)$$

$$\text{Momentum conservation: } P - P_0 = \rho_0 D u \quad (1.23)$$

$$\text{Energy conservation: } P u = \frac{1}{2} \rho_0 D u^2 + \rho_0 D (E - E_0) \quad (1.24)$$

A fourth relation is the equation of state that brings the description of the mater under a thermodynamic state  $(P, \rho, E)$ . A closure relation, equation (1.25), describes the dependency of the shock velocity  $D$  with the material velocity  $u$ , where  $C_0$  and  $s$  are characteristic constants of the material that can be determined experimentally.  $C_0$  is also referred to as the hydrodynamic speed of sound and can be calculated based on equation (1.26), where  $C_L$  and  $C_T$  are the longitudinal and transversal speed of sound.

$$D = C_0 + s \cdot u \quad (1.25)$$

$$C_0 = \sqrt{C_L^2 - \frac{4}{3} C_T^2} \quad (1.26)$$

For isotropic materials, the longitudinal speed of sound can be estimated based on the elastic modulus of the material ( $E$ ) and its initial density  $\rho_0$  using equation (1.27). However, composite materials have orthotropic properties, hence the same equation cannot be used. For unidirectional composites, the longitudinal speed of sound in the fiber direction can be determined using equation (1.28), while the longitudinal speed of sound in the direction perpendicular to the fiber can be calculated using equation (1.29) [36], [81].

$$C_L = \sqrt{\frac{E}{\rho_0}} \quad (1.27)$$

$$C_L = \sqrt{\frac{E_{11}}{\rho_0(1 - \nu_{12}\nu_{21})}} \quad (1.28)$$

$$C_L = \sqrt{\frac{E_{22}}{\rho_0(1 - \nu_{12}\nu_{21})}} \quad (1.29)$$

### 1.4.3 Tensile stress generation and velocity signal analysis for failure diagnosis

Fig. 1.2a illustrates the shockwave propagation in the time-position plane for the analytical representation of the phenomena and also the Pressure versus Particle velocity diagram (shock polar), in the case of no damage in the material.

Depending on the material properties (impedance, thickness, etc.), the two release waves can intersect inside the material thickness, resulting in a state (3) with negative pressure. The crossing of these two waves can induce a local high tensile loading which could damage the material if the stress level exceeds the material damage threshold. From this point on, if the material is damaged, voids are created inside the material, adding an inner free surface that will affect wave propagation. Therefore, the two shockwaves propagate back and forth in the two separated sections of the material, as illustrated in Fig. 1.2b.

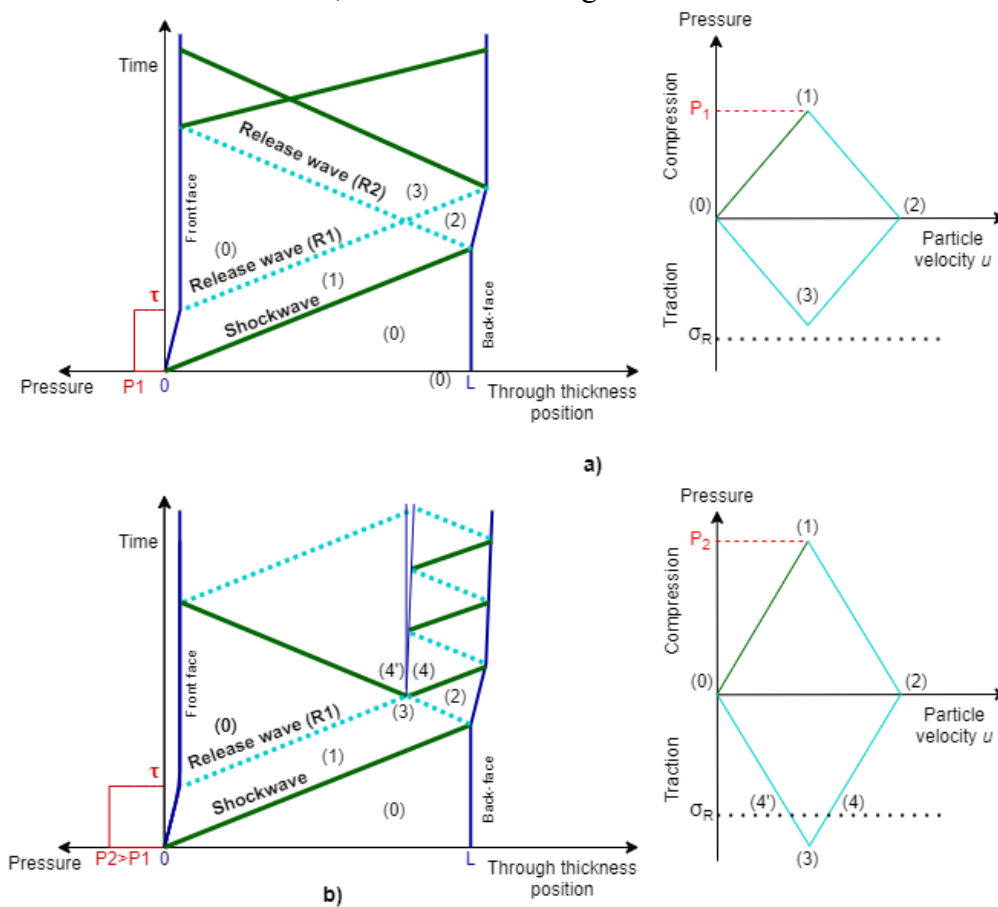


Fig. 1.2. Time-Position diagram of shockwave propagation through material thickness (left) and Pressure - Particle velocity diagram (right); a) no spall; b) spall

The two states -undamaged and damaged, can be highlighted without the need for damage inspection, with the use of back-face velocity measurement. The principle is very simple: each time the shockwave reaches the back face, a peak in the velocity measurement can be observed. An example is given in Fig. 1.3, where the back-face velocity measurement is illustrated in parallel with the Time-position diagram, for a better understanding of the correlation between the measurement and the shockwave propagation.

In the case of an undamaged sample, the two peaks exemplified in Fig. 1.3a represent the first and the second shock breakout. The time period  $t_1 - t_3$  represents the shockwave back-and-forth propagation time. This type of test and measurement can be used to determine the propagation speed of the shockwave using equation (1.30).

$$C_L = \frac{2L}{t_3 - t_1} \quad (1.30)$$

In the second case, displayed in Fig. 1.3b, the tensile stress generated at the crossing of the release waves exceeds the strength of the material, and spallation of the material occurs. The wave that propagates in the spall has a much smaller period, therefore velocity peaks in the back-face velocity measurements are more frequent than in the case of no spall.

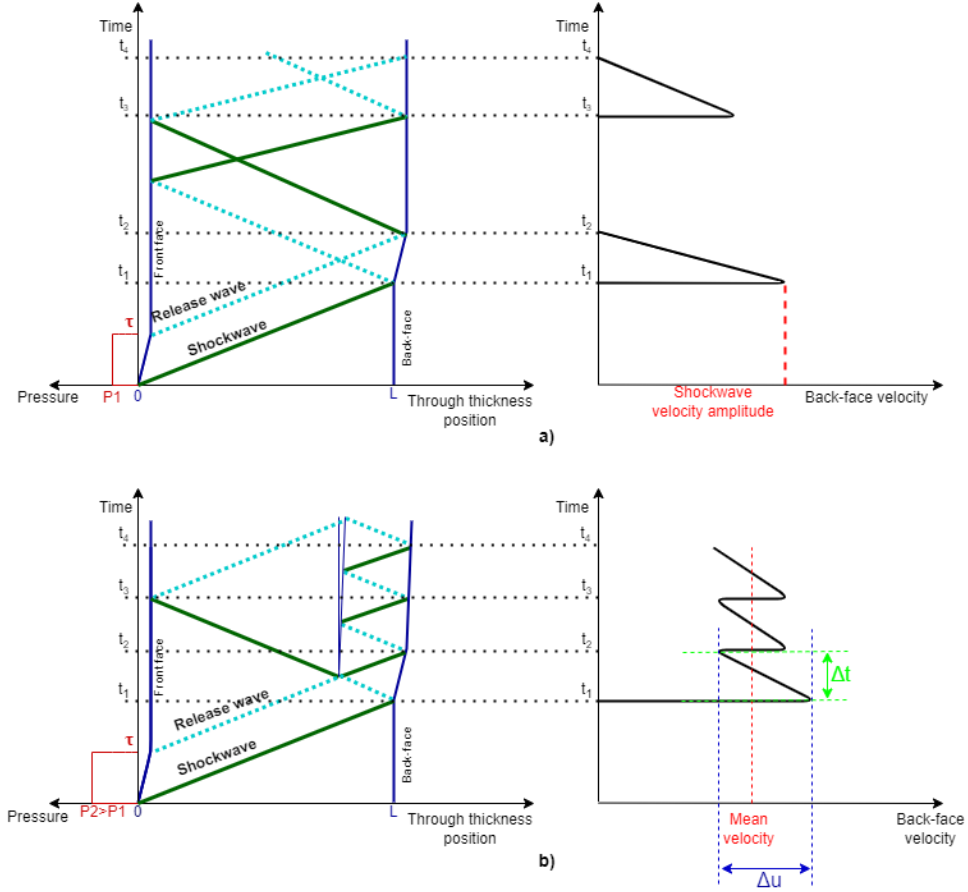


Fig. 1.3. Time-Position diagram of shockwave propagation through material thickness and corresponding back-face velocity measurement; a) no spall; b) spall

The dynamic tensile strength  $\sigma_{spall}$  can be evaluated within a homogenous material by equation (1.31), according to Novikov and Divnov [82], where  $\rho_0$  – initial density of the material and  $C_0$  – the sound velocity in the material and  $\Delta u$  represents the velocity pullback – the velocity gap measured between the maximum velocity of the first peak and the take-off point (the free-surface velocity just before the arrival of the spall pulse), illustrated in Fig. 1.3.

$$\sigma_{spall} = \frac{1}{2} C_0 \cdot \rho_0 \cdot \Delta u \quad (1.31)$$

The strain rate during delamination of the composite sample can also be estimated using the velocity pullback  $\Delta u$  [13], with the use of equation (1.32).

$$\dot{\epsilon} = \frac{1}{2C_0} \cdot \frac{\Delta u}{\Delta t} \quad (1.32)$$

#### 1.4.4 Back-face velocity measurement techniques

The measurement of the back-face velocity is of great interest for laser-induced shockwaves because it helps the understanding of the shockwave propagation through the material. It also offers information to be able to discriminate an unharmed sample from a spallation process during the shock experiment.

There are various methods of measurement based on the emission and reception of a laser beam. The most common methods are the Velocity Interferometer System for Any Reflector (VISAR)[83] and the Photon Doppler Velocimetry (PDV) [84].

The VISAR system is a time-resolved velocity measurement system that uses laser interferometry to measure the surface velocity of solids moving at high speeds.

Photonic Doppler velocimetry (PDV), also known as heterodyne velocimetry, is essentially a fiber-based Michelson interferometry and combines Doppler shifted light from a moving reflector with a reference source ( $\lambda_0 \approx 1550$  nm), yielding a complete fringe when the reflector moves a distance  $\lambda_0/2$ . Therefore, the sample reflectivity influences the measurements.

#### **1.4.5 Fiber-reinforced composites response under laser-induced shockwaves**

The development of the LASAT technique led to several studies of composite behavior under short and ultra-short shocks. Gay [85] studied the propagation of shockwaves between the different layers of a carbon fiber composite, in the through-thickness direction, and the resulting delamination. In the context of studying adhesive assemblies and detecting weak joints, Ecault [69] has shown a lot of interest in the behavior of composite materials under shocks in his thesis, both experimentally and through numerical simulations using LS-Dyna. Controlled delamination in carbon fiber composites using a symmetrical laser shock configuration was performed by Ghrib et al. [71] and laser-induced shockwave was also used as a delaminator for UHMWPE composites by Alil et al. [13]. In a more recent study, Scius-Bertrand [86] used the LASAT technique for controlled delamination and disassembly of bonded composites

Most numerical modelling of laser shock experiments on composite materials were validated only through the comparison of the computed free surface velocity and the measured one in the out-of-plane direction. This approach does not consider shock propagation along fibers and although it helps determining some mechanical characteristics, it is required to better understand shock propagation and consecutive damage in composite materials. Especially, recent studies focusing on the in-plane dynamic response of unidirectional carbon-fiber composites under laser-induced shockwaves are lacking.

#### **SUMMARY**

The first chapter of this thesis serves as a comprehensive review of the existing literature on composite materials, their hybridization and mechanical behavior, and offers a theoretical foundation on the key aspects related to characterizing fiber-reinforced composites under different loading conditions.

Among fiber-reinforced composites, those based on carbon fibers stand out as particularly suited for application in aerospace structures. While improved mechanical properties accompany higher-quality carbon fiber composites, they also come with elevated costs. To strike a balance between cost-effectiveness and technical proficiency, the concept of hybridization has gained considerable attention. Extensive research has investigated the effects of glass-carbon fiber hybridization on composite laminates, yet studies on all-carbon fiber hybrid composites remain limited. A recent innovation introduced the ply-level hybridization technique for all-carbon composites, involving the combination of prepregs with differing ply thicknesses to enhance the failure response of thin-ply composites.

While assessing the properties of composite materials designed for aerospace purposes, an evaluation of their dynamic response becomes imperative alongside their quasi-static characteristics. The laser-induced shockwave technique proves itself an appropriate and dependable approach to characterizing the dynamic behavior of composites under very high strain rates and pressures encountered in high-speed impact situations. Additionally, it allows for the assessment of the dynamic tensile strength of fiber-reinforced composites.

## CHAPTER 2. TECHNICAL PERFORMANCES MEASUREMENTS OF THE MATERIALS

### INTRODUCTION

The second chapter focuses on the materials employed in the research, with the purpose of an as complete as possible description of the materials used in this study and to provide a thorough characterization of the properties and the internal structure of the ply-level hybrid carbon/epoxy unidirectional composites with  $0^\circ$  layup. Physical properties such as density, fiber weight, and volume fraction are measured, while the internal structure of the composites is observed microscopically to identify potential defects induced by hybridization and the manufacturing process. Furthermore, an estimation of the void content is conducted to validate the laminate quality in terms of void content. This assessment aims to determine whether the void content is sufficiently low to not impact the mechanical properties of the tested laminates.

The chapter follows this structure: the first section describes the composite material configurations used in this study, covering both reference and hybrid laminates. The second section outlines the experimental testing methods and data processing techniques. The third section presents the experimental results, followed by a concluding summary at the end of the chapter.

### 2.1 MATERIALS AND LAMINATE CONFIGURATIONS

Two types of unidirectional carbon fiber preregs, having different carbon fiber types and ply thicknesses are used to manufacture the composite laminates: HSC-500-DT102S-40EF and UTS-150-DT120-32F, which will further be referred to as HSC and UTS preregs, based on the name of their carbon fiber type.

Besides the difference in thickness, the major difference in the quality of the preregs, hence on their price, relies on the fact that one has a standardized fiber, with well-known mechanical properties, while for the other prepreg, the fiber is not standardized, therefore only the minimum potential values of its mechanical properties are given by the manufacturer. Both reference materials, manufactured from only one type of prepreg, and hybrid configurations, in which the two types of preregs are combined, are manufactured.

To achieve ply-level hybridization in both ply thickness and material type, for an unsymmetric, thinner laminate denoted as H1 material, a stacking sequence of 2HSC+1UTS+1HSC+1UTS [ $0^\circ$ ] was employed. For a symmetric, thicker laminate referred to as H2 material, a stacking sequence of 1HSC+1UTS+2HSC+1UTS+1HSC [ $0^\circ$ ] was adopted. The stacking sequence of the hybrid laminates was initially determined, and based on the estimated areal weight provided by the preregs' data, the number of plies for the UTS type laminates was chosen to match the areal mass and laminate thickness of H1 and H2 samples as closely as possible. Consequently, laminates consisting of 13 and 17 UTS plies were manufactured and labeled as UTS13 and UTS17, respectively. As the HSC prepreg has thick plies and a high areal mass, the laminates were manufactured by using the number of HSC plies within each type of hybrid laminate, to assess if there is a difference in the mechanical behavior by just adding two additional UTS plies. The HSC laminates were constructed with 3 and 4 plies and will be referred to as HSC3 and HSC4, respectively.

The six different laminate configurations are illustrated in Fig. 2.1.

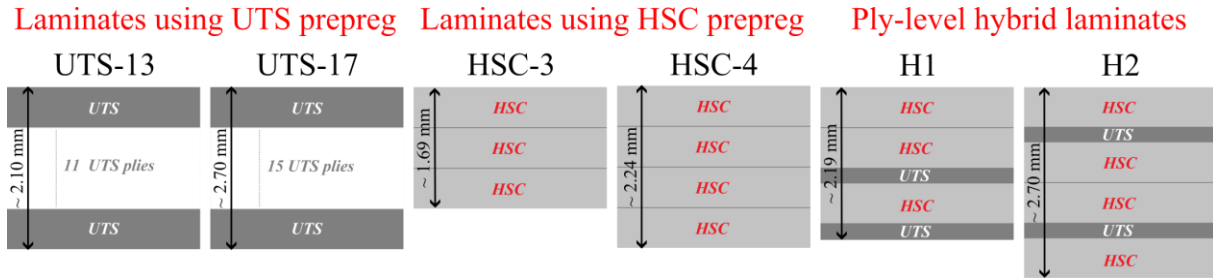


Fig. 2.1. Illustration of the stacking sequence of the manufactured laminates

## 2.2 EXPERIMENTAL METHODS AND DATA ANALYSIS

### 2.2.1 Density measurements

The density of the composite samples was measured using two approaches: a method using a laboratory scale and Archimedes' principle, and another using the mass and volume measurements of the samples. Moreover, a theoretical density is estimated using the data from the prepreg's datasheet.

### 2.2.2 Fiber weight fraction and fiber volume fraction

To determine the fiber weight and volume fraction, the burn-off method is used. The composite samples were weighed before burn-off and after, to determine the initial mass  $M_i$  and the final mass of the fibers  $M_f$ . For the test, each sample was put in a Duran glass container in a muffle furnace, at 400°C for 3h-5h, depending on the laminate type. The temperature was selected to keep the carbon fibers undamaged and to also be in the recommended temperature range of the glass container.

### 2.2.3 2D Microscopic Observations

For microscopic observations of the structure of the laminates, rectangular samples with a length of 25 mm were cut from different regions of the composite plates. The composite cross-section observations were performed using a Keyence VHX-5000 series digital microscope. The samples must be prepared and thoroughly polished to have a clean image without scratches. First, the sample was fixed in a mold and embedded in cold-curing resin. ®. After the resin was cured, the samples were polished using a LaboPol-30® and LaboForce-100® polishing system from Struers®. Both annular and coaxial lighting types were used during observations, depending on which gave better results for the observed samples. Voids were analyzed using coaxial lighting, to avoid mistaking them for resin pockets and vice versa.

### 2.2.4 Void content estimation

Voids in composite materials are considered one of the most harmful manufacturing defects, as an increased percentage of voids can affect the mechanical properties of the fiber-reinforced material. Because prepreps and autoclave curing were used in the manufacturing process, a low void content is expected. Therefore, for better accuracy and the ability to investigate the position and shape of voids within the composites, 2D digital microscopy and image processing is employed. For this, microscopic images of the samples under coaxial light were saved and further processed using ImageJ software. In this 2D approach, the void content is estimated as an area fraction of the entire face of the sample.

## 2.3 EXPERIMENTAL RESULTS AND DISCUSSION

### 2.3.1 Density measurements

The mass and volume method has a higher variability in data, with a higher error bar compared to Archimedes' principle method. The main cause of the higher error for the mass

and volume method is considered to be the fact that due to the cutting process and the small dimensions of the samples, the edges are not perfectly straight and parallel, which induces an error in sample geometry measurements, therefore affecting the volume calculation. Thus, the density measurements by Archimedes' principle were considered more reliable and were used in further calculations in which the density of the laminates was needed.

By Archimedes' principle, the tested laminates have similar densities, within the interval [1.478; 1.499] g/cm<sup>3</sup>, being in the range of the theoretical density interval. A maximum difference of 1.42% was found between the densities of H1 and H2, which are the lowest and respectively the highest ones.

### 2.3.2 Fiber weight and volume fraction

After the burn-off procedure, the rectangular samples preserved their shape until they were manually manipulated. The fibers broke apart with ease from each other and were flexible. The average fiber weight fraction for all laminates is in the interval  $W_f = [59; 65]\%$ , with HSC laminates having the lowest fiber weight fraction and UTS laminates the highest one, as expected from the prepreg datasheet. The hybrid laminates H1 and H2 have in-between values compared to HSC and UTS laminates, with H2 laminate having a fiber weight fraction higher than H1 by 2%.

Regarding the fiber volume fraction, the measured values for all laminates are within the interval  $V_f = [49; 54]\%$ , having the same order as for the fiber weight fraction. By relating the density of the composites to their corresponding fiber volume fraction, the values are within the theoretically established interval.

### 2.3.3 Microscopic observation

#### 2.3.3.1 Microscopic observations on HSC laminates

The thick HSC plies can be easily identified due to the resin-rich area at the interface between the plies. Moreover, ply waviness was observed in all HSC samples, with ply thickness variation. From multiple measurements in random positions, the HSC ply thickness varies between 510-600  $\mu\text{m}$ , compared to the expected thickness from the prepreg datasheet, of 560  $\mu\text{m}$ . Both intraply and interply voids were observed within the laminates, having an almost circular shape, with dimensions ranging from 71-521  $\mu\text{m}$  for the observed samples. Regions of resin-rich areas and ply-mixing were also observed, with localized low fiber volume fraction. Fig. 2.2a shows the assembly of microscopic images of a representative HSC3 sample, with a close-up section in Fig. 2.2b.

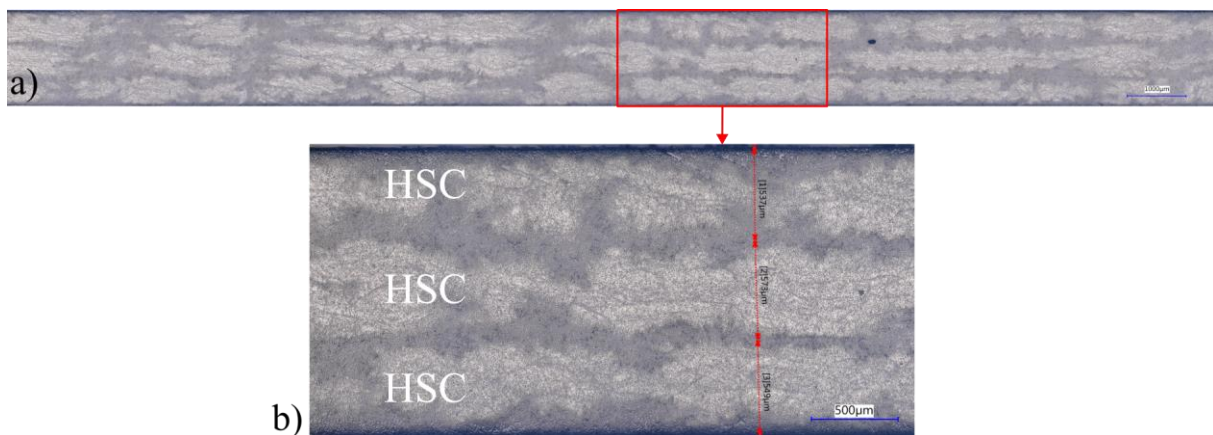


Fig. 2.2. Microscopic observation of HSC3 sample under coaxial lighting; a) view of entire sample; b) close-up view of the highlighted region with plies stacking sequence and thickness measurements

### 2.3.3.2 Microscopic observations on UTS laminates

Having thinner, more compact plies, less ply waviness was observed for UTS laminates compared to HSC laminates. Still, the ply thickness varies within the laminates, ranging from 130  $\mu\text{m}$  to 178  $\mu\text{m}$  compared to an expected ply thickness of 140  $\mu\text{m}$ . Moreover, the fiber distribution is more uniform and no regions of localized low fiber volume fraction were observed.

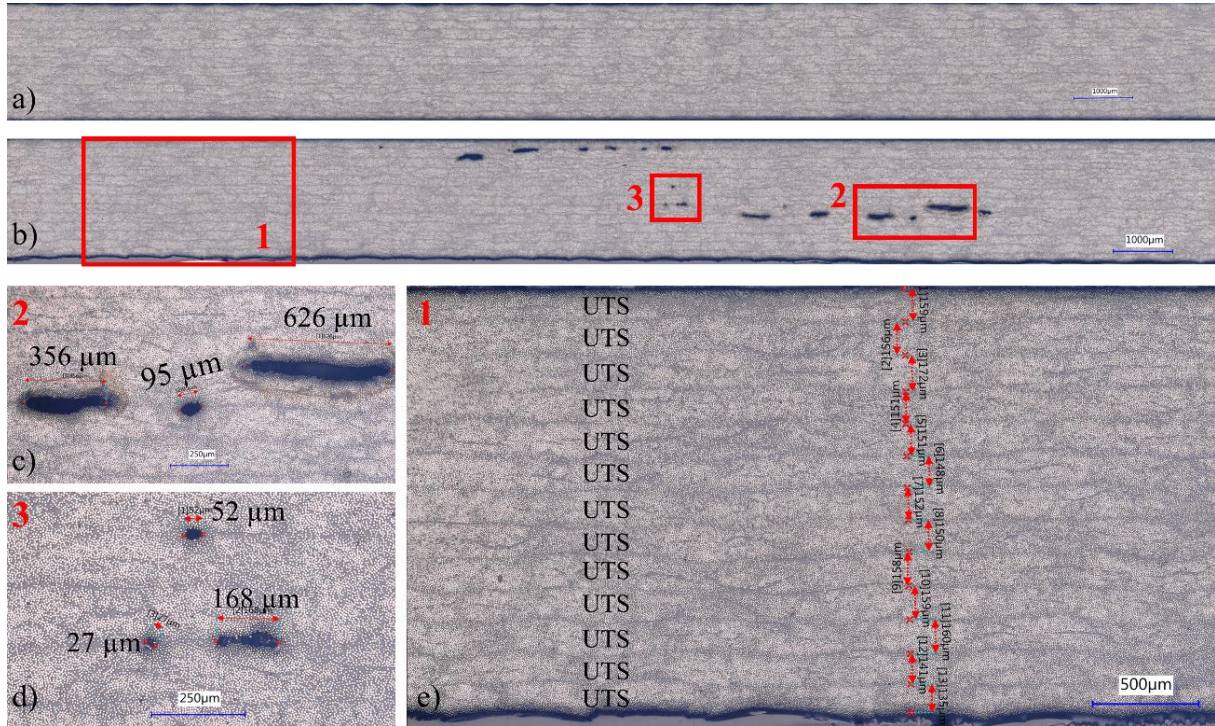


Fig. 2.3. Microscopic views of UTS13 samples under coaxial lighting; a) assembly for UTS sample free of voids; b) assembly view of UTS sample with multiple interply voids; c) close-up view of region 2 with voids dimensions measurements; d) close-up view of region 3 with voids dimensions measurements; e) close-up view of region 1 with plies stacking sequence and thickness measurements

In Fig. 2.3a, a representative UTS13 sample free of voids is presented while in Fig. 2.3b, a sample with multiple interply voids is shown. When comparing UTS laminates to HSC laminates, it is observed that UTS laminates contain more interply voids, rather than intraply voids.

### 2.3.3.3 Microscopic views on H1 and H2 sample

By analyzing the microstructure of the two types of plies within the H1 composite laminate, a significant difference in the degree of heterogeneity between thick and thin plies was observed for all samples. While the UTS plies exhibit very few resin-rich regions, thus having a more even distribution of the fibers and a uniform distributed microstructure, the HSC plies have significantly more in-ply resin-rich regions, including resin pockets and small voids.

Fig. 2.4 illustrates the microscopic observations of an H1 sample under annular lighting.

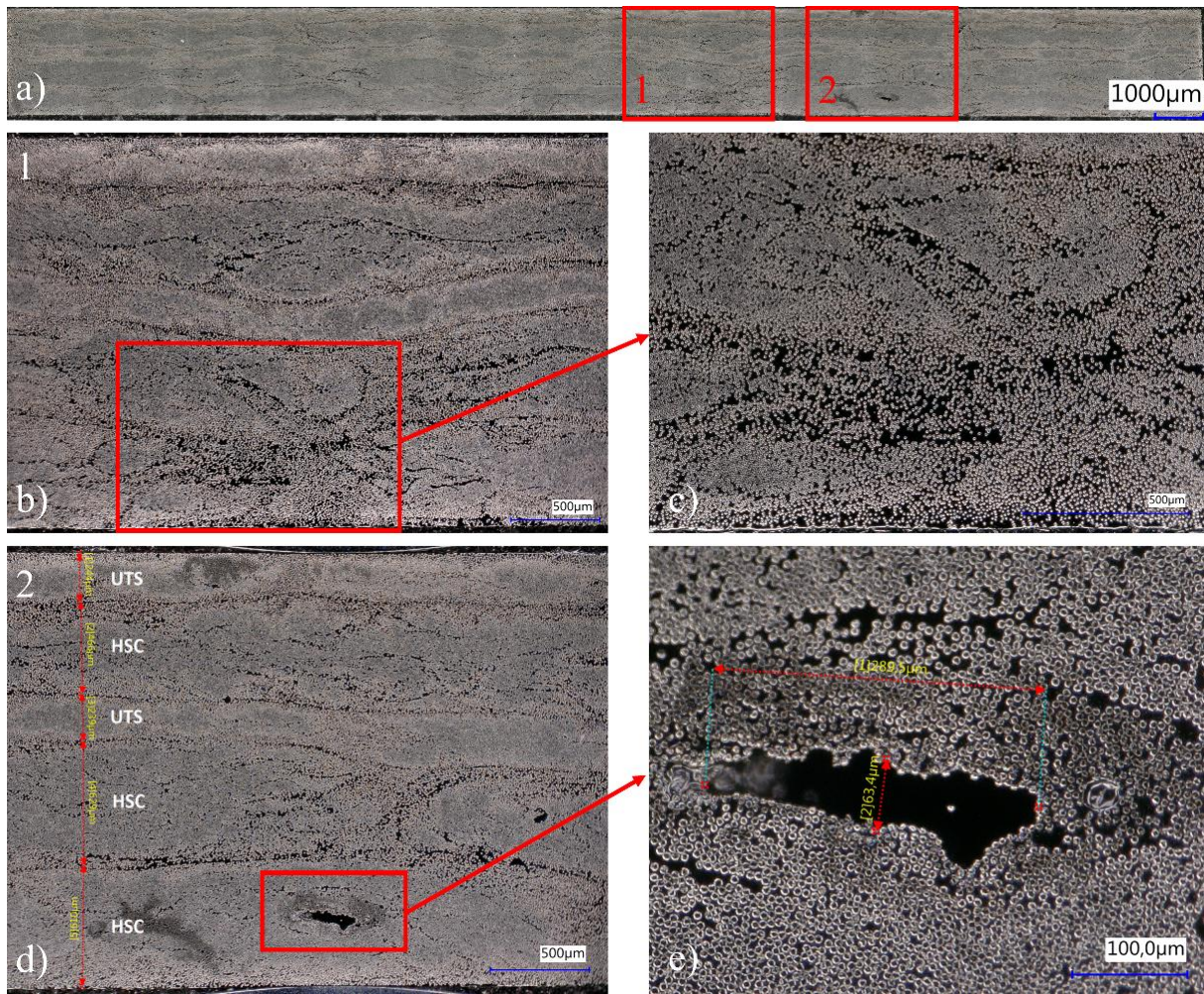


Fig. 2.4. Microscopic observations of H1 sample under annular lighting; a) assembly of the entire sample, b) resin-rich area and ply waviness, c) zoom on resin-rich area, d) laminate stacking sequence and thickness measurements, e) zoom on void with 289.5  $\mu\text{m}$  in length

While the overall thickness of the sample is mainly preserved, with only slight differences, it was observed that all the samples show ply waviness. It is considered to appear due to the thicker prepregs used [87]. Also, HSC laminates showed increased ply waviness compared to UTS laminates. Moreover, the waviness at the interface between the two adjacent HSC plies is more severe when compared to the waviness of the HSC ply placed between the UTS plies.

### 2.3.4 Void content estimation

The average void content for the tested laminates is presented in Table 2.1. Because the void content estimation based on 2D micrography images is section-biased, there is high variability in the void content of the individual samples for each laminate configuration leading to very high standard deviations.

Table 2.1. Average void content and standard deviation

Material	UTS13	UTS17	HSC3	HSC4	H1	H2
Average void content [%]	0.228	0.243	0.007	0.097	0.017	0.220
Standard deviation [%]	0.295	0.194	0.008	0.105	0.015	0.086

For all the composites under scrutiny, the estimated void content remained below 1%, which is indicative of good composite quality. This low void content suggests that the mechanical properties of these composites should remain unaffected by voids.

## SUMMARY

In this chapter, objective 1 was attained, and an experimental characterization of the internal structure and physical properties of both reference and ply-level hybrid unidirectional carbon fiber composites was carried out, contributing to the main objective of the thesis.

To realize this, the ply-level hybridization technique was adapted, which allowed to achieve hybridization not only in ply thickness but also in material quality. This was accomplished by combining high-quality carbon fiber prepreg plies with plies of lower quality within the same laminate. Two distinct stacking sequences for the hybrid laminates were explored: one symmetric by the midplane and the other unsymmetric. In addition, the creation of reference laminates served the dual purpose of establishing a foundational benchmark for comparing the hybrid laminates and facilitating a comparison between UTS and HSC laminates.

With a volume fraction ranging from 49% to 54%, the densities of the composites, determined using Archimedes' principle, exhibited similar values, with a maximum difference of only 1.42%. Archimedes' principle-based density values were identified as more reliable, and thus, they will serve as the basis for subsequent calculations requiring the density of the tested composites.

Microscopic observations revealed distinct characteristics of the UTS composites compared to the HSC counterparts. UTS composites demonstrated greater uniformity in their plies and reduced ply waviness, although they exhibited a higher percentage of interply voids compared to HSC composites. The internal structure analysis of the hybrid laminates indicated improvements in terms of ply mixing, resin-rich regions, and ply waviness when contrasted with HSC laminates. For all the composites under scrutiny, the estimated void content remained below 1%, which is indicative of good composite quality. This low void content suggests that the mechanical properties of these composites should remain unaffected by voids.

## CHAPTER 3. QUASI-STATIC BEHAVIOR OF PLY-LEVEL HYBRID CARBON COMPOSITE MATERIAL

### INTRODUCTION

This chapter provides a comprehensive analysis of the quasi-static mechanical performance of hybridized composite materials in comparison to high-standard reference materials. The main aim is to ascertain their suitability for cost-effective applications in the aerospace industry. Throughout this chapter, objectives 2, 3, and 4 are addressed.

The performance evaluation from a mechanical point of view involves monotonic on and off-axis quasi-static tests, conducted at a controlled displacement rate of 1 mm/min, to assess the in-plane behavior of both hybrid and reference laminates. On-axis tensile tests are carried out to determine in-plane properties, while off-axis tests reveal the nonlinear stress-strain behavior with varying off-axis angles. The impact of thickness on off-axis mechanical responses is also investigated, using reference laminates with different thicknesses.

For strain analysis, Digital Image Correlation is employed, supplemented by a successive linear regression method to assess the apparent Young modulus in off-axis samples, due to the nonlinearity of the stress-strain response.

Cyclic load-unload off-axis testing is undertaken to uncover the origins of nonlinear responses, and methods for residual strain and damage variable estimation are employed. Moreover, parameters required for nonlinear constitutive models are estimated, and predictions of off-axis behavior are carried out using a nonlinear coupled damage-plasticity model, offering insights into the predictive capabilities of the approach.

The chapter's subsequent structure comprises detailed accounts of the experimental methodologies, followed by the presentation and analysis of results for each test type. Additionally, discussions explore the particularities of the tested laminates and the effects of hybridization.

### 3.1 MATERIALS AND METHODS

#### 3.1.1 Experimental setup

Quasi-static tension tests are performed to determine the on and off-axis response of the unidirectional laminates for three different fiber orientations: 15°, 30°, and 45°. Guidelines from EN ISO 527-5 [33] standard were followed to conduct these tests. All mechanical tests were carried out at ambient temperature (20° C) and controlled in displacement at 1 mm/min. The strain rate is approximated by dividing the crosshead displacement rate by the gauge length of the sample (~150mm), yielding an approximate strain rate of  $10^{-4} \text{ s}^{-1}$ .

Most 0° tensile tests were carried out on an ADAMEL® Lhomargy DY36 testing machine at ENSTA Bretagne with a load cell of 100 kN and wedge grips. Part of H1 and HSC3 0° tensile tests and all 90° and off-axis tensile tests were performed with an electromechanical testing machine INSTRON® 5960, with a load-cell of 50 kN and wedge grips, also at ENSTA Bretagne.

Strain measurements were performed with the use of Digital Image Correlation (DIC). GOM Aramis® 5M was used for most DIC measurements, post-processing, and extraction of the strain values. For part of the H1 0° tensile tests, a simple Retiga® 1300 camera was used to

record the images, and GOM Correlate® Software for post-processing and extraction of the strain values, as the GOM Aramis® 5M was unavailable at the time of the experimental tests. However, the setup only allowed for half of the laminate’s gauge length to be in the DIC system field of view.

### 3.1.2 Sample description and preparation

The dimensions for the 0° test are shown in Fig. 3.1a, while for the 15°, 30°, 45°, and 90° tests, the sample dimensions are presented in Fig. 3.1b. Corresponding axis systems are designated as follows: X – the load direction, Y – transverse to the load direction, 1 – fiber direction, 2 – transverse to the fiber direction, and  $\theta$  – the off-axis angle. In the case of the 0° tensile test, H1 samples exhibited a width of approximately 11 mm, while the width for all other laminates was around 15 mm. To reduce the gripping effects, aluminum tabs were bonded on the specimens using an Araldite 420 A/B Epoxy Adhesive System.

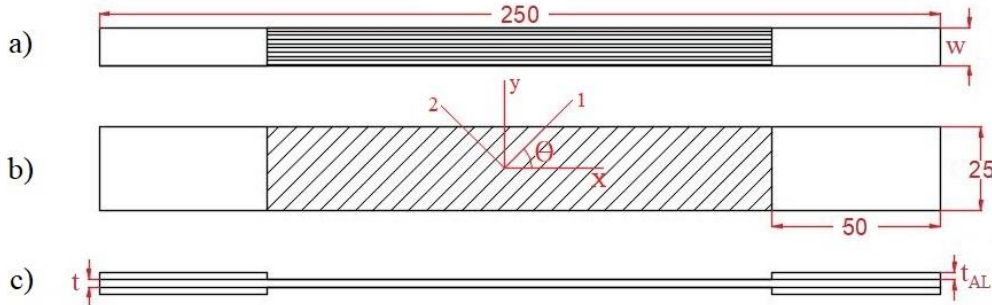


Fig. 3.1. Samples dimensions in mm; a) 0° tensile test b) off-axis and transverse tensile test c) side view of samples; all dimensions are in mm, w – width of the sample, t – thickness of the sample,  $t_{AL}$  – thickness of aluminum tabs

### 3.1.3 Data processing

MATLAB® software was used for the linear fit and data extraction for both the Young modulus and Poisson ratio from stress-strain curves extracted from DIC analysis,

For off-axis tensile tests, which exhibit a nonlinear stress-strain response, a successive linear regression method was proposed and employed for the evaluation of the apparent Young modulus in off-axis samples. This method offers the advantage of minimizing errors induced by the manual selection of the data in the linear response region of the off-axis stress-strain response. The schematic diagram of this method is detailed in Fig. 3.2.

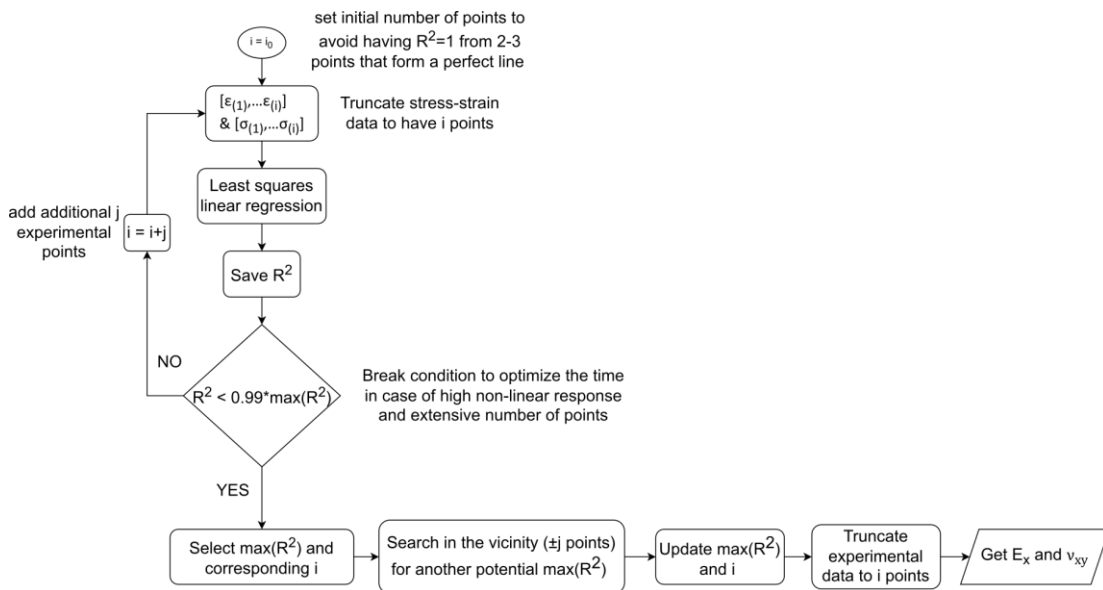


Fig. 3.2. Flowchart of the successive linear regression procedure on stress-strain relations obtained from experimental data extracted with DIC

## 3.2 EXPERIMENTAL RESULTS AND DISCUSSION

### 3.2.1 On-axis tensile tests – 0° and 90°

The in-plane tensile properties of the manufactured composites were obtained from quasi-static tensile testing. No thickness effects were noticed on the stress-strain response under both longitudinal and transverse quasi-static tensile loading. For equivalent thickness and sample geometry, hybrid composites exhibited an improved 0° failure stress compared to the estimated strength based on Kawai's scaling function. Failure for tensile tests in the fiber direction was in the form of longitudinal splitting with ultimate fiber failure at the end tabs.

For the transverse failure stress, high dispersion of data was obtained because most samples failed close to the grips (~ 4 out of 7 samples). The in-plane properties of the studied materials are similar to other published works performed on similar unidirectional carbon fiber-reinforced composite materials [88]–[92].

### 3.2.2 Off-axis tensile tests

Fig. 3.3 shows the stress-strain response under uniaxial tension at various angles for all material configurations. The response for the 0° test was truncated to have a clearer view of the response at the other angles. Each material shows an increased nonlinear response with decreasing off-axis angle. Furthermore, there is a reduction in the apparent elastic modulus as the off-axis angle increases. In the linear response region, minor differences were observed among the laminates, while in the nonlinear response region, the HSC laminates demonstrated strain hardening compared to the UTS laminates, but had a smaller failure strain. Both hybrid laminates exhibited higher failure stress levels compared to simple laminates and had intermediate failure strains.

For the ultimate strain reached, there is a downtrend with increasing angle, except the 30° test for which, both in individual and averaged comparison, the ultimate axial strain reached is higher than for the 15°. The lowest ultimate strain is for  $\theta=90^\circ$ , as expected.

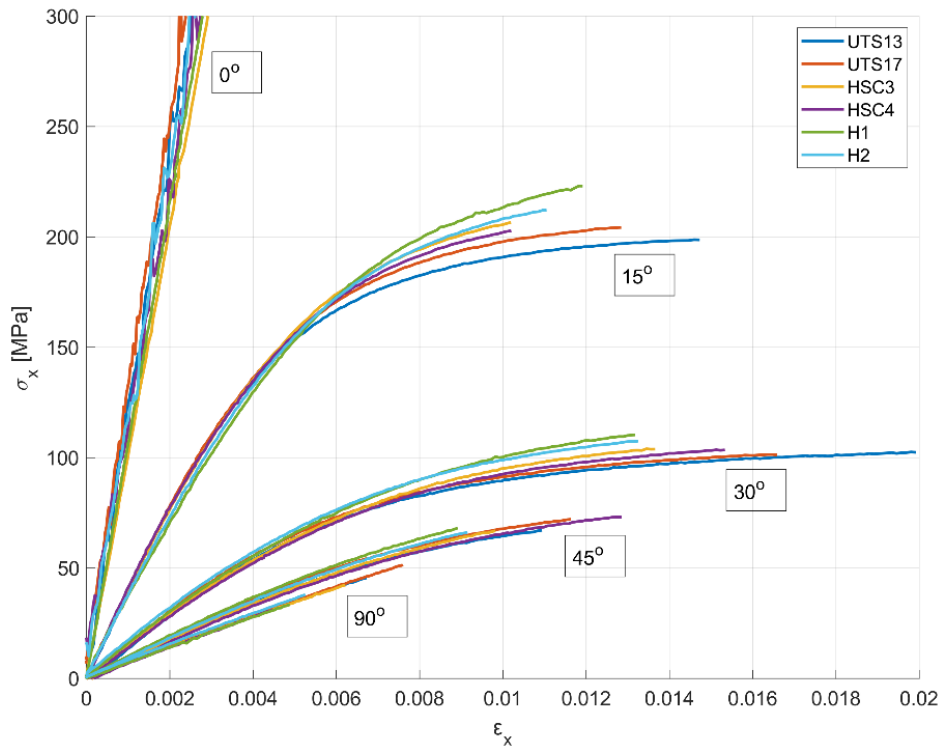


Fig. 3.3. Stress-strain curves obtained by DIC of on and off-axis specimens at 1 mm/min

No significant thickness effects were observed in the stress-strain response during quasi-static off-axis tensile loading within the linear response region. However, slight differences in

stress levels were noted for laminates with the same material but different thicknesses in the nonlinear response region.

The experimental results revealed a degradation of off-axis elastic moduli with increasing off-axis angles, in accordance with predictions using the transformation equation. Similar degradation was observed in the off-axis strength. The in-plane shear modulus was evaluated using tensile tests at various off-axis angles, and the modulus extracted from the 45° off-axis test was selected for further calculations, following the recommendations of Pindera et al. [37].

### **3.2.3 Damage assessment by Cyclic Load-Unload tensile tests**

Furthermore, cyclic load-unload off-axis testing was performed to investigate the cause of the nonlinear response. After analyzing the results, it was concluded that the nonlinearity is caused by a combination of internal damage and residual strain. The evolution of the damage variable and the accumulated residual strain were quantified by analyzing the incremental loading/unloading stress-strain response of the tested samples. Overall, UTS laminates have the highest residual strains in all test cases, suggesting that the matrix in UTS prepreg has an inherent higher plasticity characteristic compared to HSC laminates, while the hybrid laminates have the smaller residual strains of all materials. For the estimation of the damage variable, three methods are used: Ladeveze, Fitoussi, and Regression. Among these methods, the Regression method is unreliable for extracting the elastic modulus of the load-unload cycles and estimating the damage variables for the materials used in this study, because the damage variable changes at an irregular rate when stress levels increase, giving also negative values and high error bars.

### **3.2.4 Predictions of off-axis nonlinear stress-strain response**

The parameters required to define a nonlinear constitutive model for predicting the off-axis behavior of unidirectional ply-level hybrid composites were determined from the residual strain and damage variable experimental data. For predictions of the off-axis behavior of the studied composites, only the damage variables given by Ladeveze and Fitoussi methods are considered.

Overall, a good prediction was obtained, with deviations from the experimental results in the nonlinear response region. By increasing the value of  $b_2$  from 0.05 to 0.2, better predictions are obtained for all laminates. Moreover, predictions for thicker reference laminates were performed using the damage and plasticity parameters from thinner laminates of the same material prepreps. Prediction results were improved for UTS17 laminate and were satisfactory for HSC4, confirming that for laminates with a thickness difference up to 0.7mm, using the same plasticity and damage parameters offers satisfactory prediction results.

Additionally, predictions of the hybrid laminates' off-axis response were made using the damage parameters of the hybrid laminates and plasticity parameters from the HSC laminates. In the nonlinear response region, the predictions were significantly improved, underlying the importance of the plasticity parameters, and suggesting that the softening in the nonlinear response region is mainly caused by the plasticity of the matrix and in the case of the tested hybrid laminates, the plastic response is mainly governed by the matrix in the HSC plies. Fig. 3.4 shows an example of the prediction of HSC4 nonlinear response, with corresponding percentage errors between the anticipated stress and the actual experimental values.

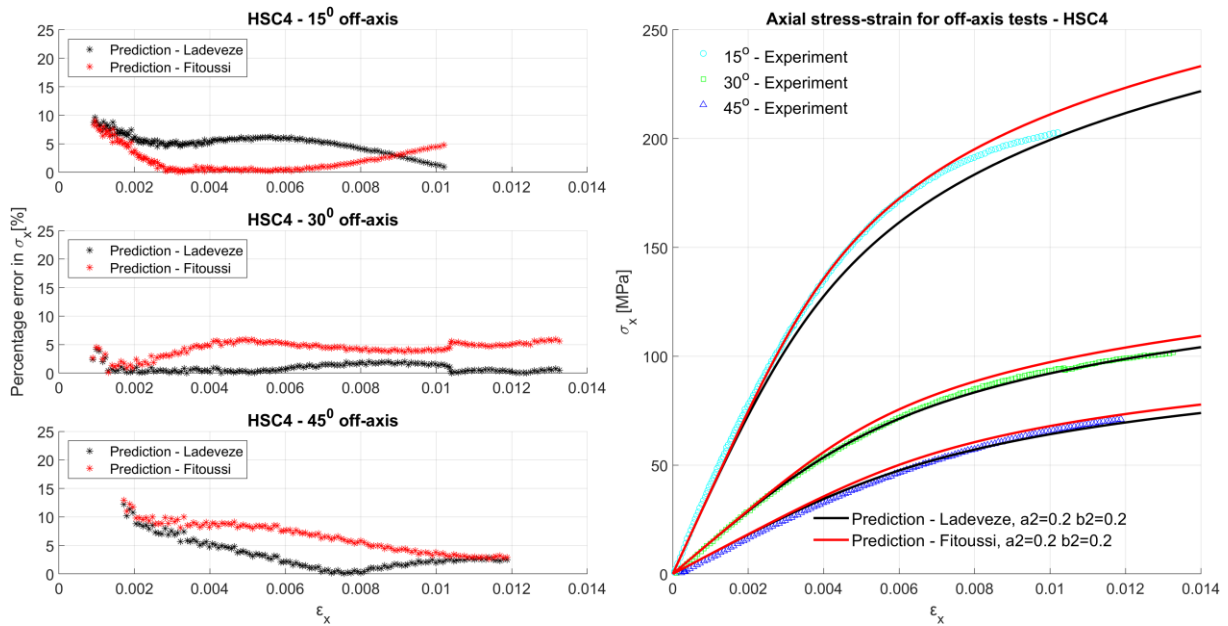


Fig. 3.4. Predictions of the off-axis nonlinear stress-strain of HSC4, with damage variable estimation from both Ladeveze and Fitoussi methods,  $a_2=0.2$  and  $b_2=0.2$  – with corresponding  $\sigma_x$  percentage error between predicted values and experimental results

### SUMMARY

This chapter aimed at evaluating the quasi-static mechanical performances of hybridized composite materials with respect to high-standard reference materials. The overall goal is to validate an economic choice based on safety justifications relying on a mechanical approach for structural applications in the aeronautic and aerospace industry. Throughout this chapter, objectives 2 (evaluate of the quasi-static mechanical response of hybrid and reference laminates under on and off-axis tensile testing), 3 (investigate the cause of the nonlinear off-axis response through off-axis cyclic load-unload tensile tests and evaluate residual strains and damage variables), and 4 (define a coupled damage-plasticity model to predict the nonlinear off-axis response of laminates) were achieved.

## CHAPTER 4. DYNAMIC RESPONSE OF PLY-LEVEL HYBRID COMPOSITE MATERIALS

### INTRODUCTION

While the third chapter is dedicated to quasi-static testing, the fourth and final chapter contains the findings related to dynamic loading under high strain rates. The complement in the dynamic regime of the mechanical characterization of the studied materials is needed for the design of aircraft structure components, as they can be subjected to intense and impulsive loadings such as mechanical impacts at high velocity. These impacts can be encountered during the rupture of a fan blade, a ballistic or warhead attack for example. In this chapter, the dynamic response at very high strain rates ( $> 10^5 \text{ s}^{-1}$ ) is evaluated. As the composite material of interest is unidirectional, this study also considers the evaluation of shockwave propagation in the fiber direction.

In this approach, in the first part of the fourth chapter, laser-induced shockwaves are chosen to produce intense and impulsive mechanical loadings. Thus, two types of laser tests are performed: one in the fiber direction (in-plane), and one perpendicular to the fiber direction (out-of-plane). The sample preparation for the laser-induced shockwaves tests as well as the experimental setup are described in this chapter. The methods used for data processing and analysis are detailed. The experimental results and discussions for each type of laser test are presented, along with an analysis of the hybrid material response compared to reference laminates.

The second part of the fourth chapter describes steel ball impact testing on one of the hybrid composite plates (H2), along with a few experimental data results. This type of test is explored to provide additional insight into damage propagation during impact with a foreign object, as well as the energy absorption capacity of the unidirectional laminates. It serves as a foundational step for future structural analyses.

### PART 1: LASER-INDUCED SHOCKWAVES

#### 4.1 SAMPLE DESCRIPTION

Because of the anisotropic aspect of composite materials, several experimental characterizations are chosen: one in the sample's out-of-plane direction and one in the in-plane direction, mainly in the fiber direction. In this intention, two types of specimens were prepared.

Small plates of approximately  $2.5 \times 5 \text{ cm}$ , with the fibers aligned with the longer edge, were used for the out-of-plane laser shock test. For the in-plane laser shock test, the thickness of the laminate plates was insufficient to accommodate the focal spot, as its diameter is about  $3.5 - 4 \text{ mm}$ . Therefore, thin stripes of  $\sim 2 \text{ mm}$  thick composite material were precision-cut using a diamond cut-off saw and were bonded on top of each other with ethyl-cyanoacrylate (glue) from Sader.

In both tests, a sacrificial layer of aluminum tape with  $50 \mu\text{m}$  of aluminum and  $30 \mu\text{m}$  of adhesive is used to have a mastered laser-matter interaction [93], [94], and also to be able to approximate the mechanical loading generated on the specimen's surface. Additionally, a reflective surface is necessary for measuring the back-face velocity. To achieve this, a thin gold layer was applied to the back face using a sputtering machine COXEM SPT-20 ION-COATER.

## 4.2 EXPERIMENTAL SETUP

The laser source is an Nd: YAG Quanta-Ray Pro 350-10 delivering a Gaussian pulse of about 7.5 ns, with a maximum energy of 3.5 J at the output in its fundamental mode at a wavelength of 1064 nm, when warmed up at 10 Hz. The energy gradation can be continuously adjusted outside the laser source with a variable attenuator comprised of a quarter wave plate and a polarizer mounted in a rotative mount, at the Brewster angle of  $56^\circ$ . This ensures that the laser is working at its maximum energy and accounts for better laser pulse repeatability. To obtain better shot parameters, the continuous 10 Hz working mode is preferred, and a previously developed mechanical shutter is set in place to reflect the laser beam into a beam dump.

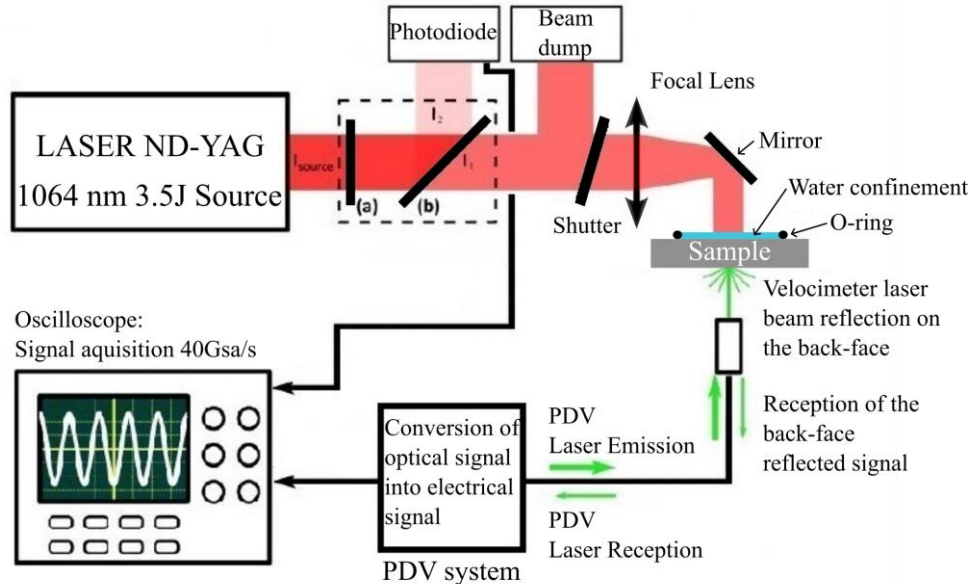


Fig. 4.1. Scheme of laser impact experimental setup (not at scale); (a) quarter-wave lens, (b) polarizer

Photon Doppler Velocimetry (PDV) manufactured by IDIL France is used for measuring the back-face velocity. The measured quantities are recorded by an acquisition chain triggered by a fast response time photodiode ( $<1\text{ns}$ ) UPD300SD distributed by Alphalas. A fast oscilloscope Agilent DSO80604B (50 Ohm, 6GHz, 40 GS/s) is used for signal acquisition. The scheme of the described experimental setup with the laser impact shot and measurement chain is represented in Fig. 4.1.

## 4.3 LASER PULSE CHARACTERIZATION

### 4.3.1 Pulse Duration and Time Shift

To measure the pulse duration of the laser shot, a fast response time photodiode UPD 300 SD (rising and falling time  $< 1\text{ ns}$ ) is used. The pulse durations of the measured Gaussian pulses are determined at half maximum - or full width at half maximum (FWHM). From 4 sets of measurements (10 for 100%, 10 for 75%, 5 for 50%, and 5 for 25%), the average pulse duration was evaluated at 7.35 ns, with a standard deviation of 0.36 ns. The obtained pulse duration is similar to the manufacturer's specification of 7.5 ns.

Due to the delay in the chain of measurement, corresponding to the delay of the information transit in BNC cables and optical fibers, a time-shift must be considered for each laser shot, to set the start of the rising laser loading at zero time. To evaluate the required time shift for each test, an analysis is performed of the rising front of the laser pulse. The time shift is calculated for each laser impact test. The actual trigger time results from the trigger level adjusted at the oscilloscope, on the rising edge of the photodiode signal. Therefore, the time scale of the corresponding back-face velocity signal is adjusted accordingly.

In addition to this correction, one shall consider the lens-target distance that differs from the lens-photodiode distance. Moreover, there is a loss of time in RG58 cables from the

photodiode to the oscilloscope ( $\sim 5$  ns/m), and in the PDV system because of the length of optical fibers ( $\sim 3$  ns/m). To estimate this time loss, a shot is preliminarily performed on an Al target of  $1000 \mu\text{m}$  thick with a known sound speed of  $5390$  m/s [95] and  $C_L=6300$  m/s.

### 4.3.2 Energy Measurements

Two laser shock experimental campaigns were performed one in 2021, mainly on H1 material, and a second one in 2022. For both campaigns, energy measurements were made using a QE25LP-S-MB-QED-D0 Pyroelectric detector for laser energy measurement coupled with a MAESTRO interface, both manufactured by Gentec.

The energy levels and corresponding angle of the polarizer and energy values in both experimental campaigns are presented in Table 4.1. All energy measurements have an uncertainty of  $\pm 0.01\text{J}$ . The values of the energy represent the energy deposited on the target.

Table 4.1. Laser energy measurements

Energy level [%]	Polarizer Angle [deg]	Energy value [J]	
		2021 Campaign	2022 campaign
100	0	2.63	2.94
85	11	2.24	-
75	14	1.97	2.22
50	22.5	1.31	1.54
35	27	0.92	1.10
25	30	0.66	0.85
15	35	0.39	-
10	36.5	0.26	-

### 4.3.3 Focal Spot Analysis

When the laser beam hits the target, a focal spot is imprinted on the target surface. The focal spot dimension influences the density of power of the shot. The use of a confinement medium improves the uniformity of the focal spot, hence the laser energy distributed to the target.

In the first experimental campaign (2021), a focal spot diameter at a maximum energy of  $4$  mm was set. In the experimental setup in the second experimental campaign (2022), the same focal spot was intended, but due to the optical chain involved, a maximum focal spot of  $3.85\text{mm}$  was obtained. Although the same experimental setup was used for shots at different energy levels (in the respective campaigns), in both cases it was observed that the focal spot decreases with the energy level. Small variations in the diameter of the focal spot were found also for shots at the same energy level.

## 4.4 HETERODYNE VELOCIMETRY

### 4.4.1 Signal Processing

For laser-induced shockwave experiments, back face velocity measurements are of high interest as this time-resolved measurement is fast enough to provide valuable information on shock propagation history, its effect on material, and velocity history. . In this intention, the Photonic Doppler Velocimetry technique was used. The PDV signal was saved after each shot and processed with Caffeine software, provided by the French institution Commissariat à l'Energie Atomique.

### 4.4.2 Speed of Sound Estimation from BFV Signals

Because a sacrificial layer is used, to determine the propagation speed in the composite laminate, equation (1.30) is adapted to account for the propagation time in the aluminum and glue layers from the aluminum tape, giving equation (4.1), where  $L$  denotes the composite thickness without the aluminum layer,  $t_{AL}$  and  $t_{GL}$  represent the propagation time in the aluminum and glue layer respectively (from the aluminum foil). For the aluminum layer the

shockwave speed is  $C_{LAL} = 6300$  m/s, and  $C_{0GL} = 1200$  m/s for glue [94]. The elastic wave in glue is neglected.

According to the shock polar in Fig. 1.2, the material velocity for the maximum pressure load is half of the maximum back-face velocity. Thus, when evaluating the speed of sound, half of the back-face velocity is subtracted from the propagation speed determined from the back-and-forth propagation. Equation (4.2) is used to estimate the speed of sound, where  $u_{BFV}$  represents the maximum velocity of the first peak in the case of in-plane laser shots, and the average value between the maximum velocity of the first and second peak in the case of out-of-plane laser shots, as the shockwave is attenuated and the maximum velocity of the second peak is significantly lower than the first one.

$$C_L = \frac{2L}{t_3 - t_1 - t_{AL} - t_{GL}}; \quad t_{AL} = \frac{2L_{AL}}{C_{LAL}}; \quad t_{GL} = \frac{2L_{GL}}{C_{0GL}} \quad (4.1)$$

$$C_0 = C_L - \frac{1}{2}u_{BFV}; \quad (4.2)$$

For the back-face velocity of in-plane samples, the number of back-and-forth shockwave propagations within the 4  $\mu$ s timeframe is much higher than for out-of-plane samples, for which only two shockwave breakouts are captured, suggesting a higher propagation speed. The shockwave is also less attenuated in one back-and-forth propagation for the in-plane shot, compared to the out-of-plane case. Therefore, to have a more accurate propagation period, a Fast Fourier Transform (FFT) analysis is used for the back-face velocity signals of in-plane samples, to extract the period of oscillation.

#### 4.4.3 Dynamic Tensile Strength and Strain Rate Estimation from BFV Signals by Novikov's approach [82]

To estimate the dynamic tensile strength (or spall strength) with equation (1.31) and strain rate during delamination using equation (1.32), back-face velocity signals that exhibit spall signal, as presented in Fig. 4.2 are selected. In this work, a spall is represented by a crack occurring in a damage plane parallel to the back face due to high dynamic tensile stress. This spall can be either a crack in the matrix or a delamination at the interply.

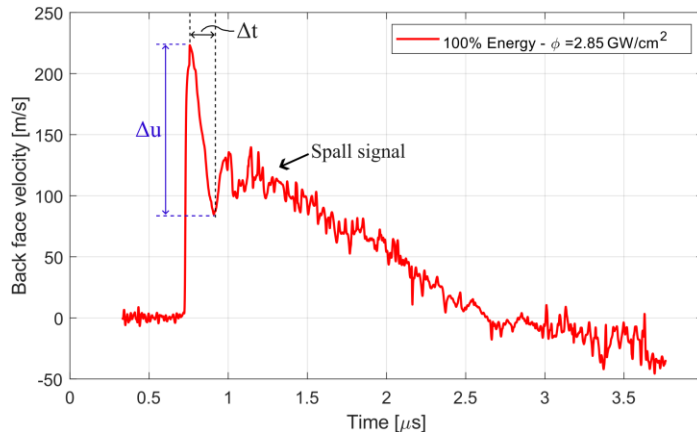


Fig. 4.2. Example of data identification for estimating the dynamic tensile strength and strain rate from a back-face velocity curve with a spall signal for a sample shot in the out-of-plane direction

#### 4.5 DAMAGE ANALYSIS PROCEDURE

To further analyze the internal damage in out-of-plane samples, diagnosed through the back-face velocity signal, microscopic observations of the sample's cross-sections were made. The samples were prepared according to the sequence of steps illustrated in Fig. 4.3.

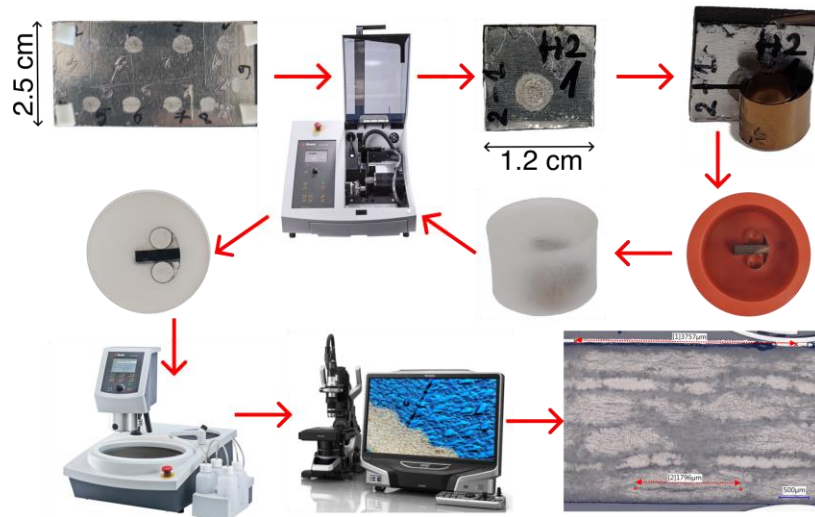


Fig. 4.3. The sequence of steps - from out-of-plane sample to microscopic observations

#### 4.6 REPEATABILITY OF EXPERIMENTS

The preliminary testing to ensure the repeatability of the experiment setup was made on a sample in the out-of-plane direction. Shots with 100%, 50%, and 10% of max energy were performed on the same plate, at a distance between shots of  $\sim 1$  cm, and the back-face velocity was recorded. It was concluded that the repeatability of the tests, regarding the peak velocities and chronology, is satisfactory. Additionally, for each testing configuration, a minimum number of two shots were performed.

#### 4.7 EXPERIMENTAL RESULTS AND DISCUSSION

##### 4.7.1 Along the fiber-direction (in-plane) laser-induced shockwave test results

###### 4.7.1.1 Back-face velocity signal analysis for in-plane laser tests

In the fiber direction (in-plane) laser impact shots were performed on the materials at three different energy levels, and by analyzing the back-face velocity signal, recorded by laser-Doppler interferometry, a decrease in the maximum velocity of the first peak with the decrease of energy level was observed. A spall signal due to the expulsion of the gold layer deposited on the back-face for increased reflectivity was noticed for two H1 samples and it slightly influenced the extraction of the back-face velocity signal.

Fig. 4.4 depicts a comparison of representative back-face velocity signals for both reference and hybrid laminates, for different energy levels. Overall, the shockwave attenuation is more pronounced in hybrid laminates than in UTS reference laminates, having a response closer to HSC laminates. This outcome was anticipated since the hybrid laminates consist predominantly of HSC fibers.

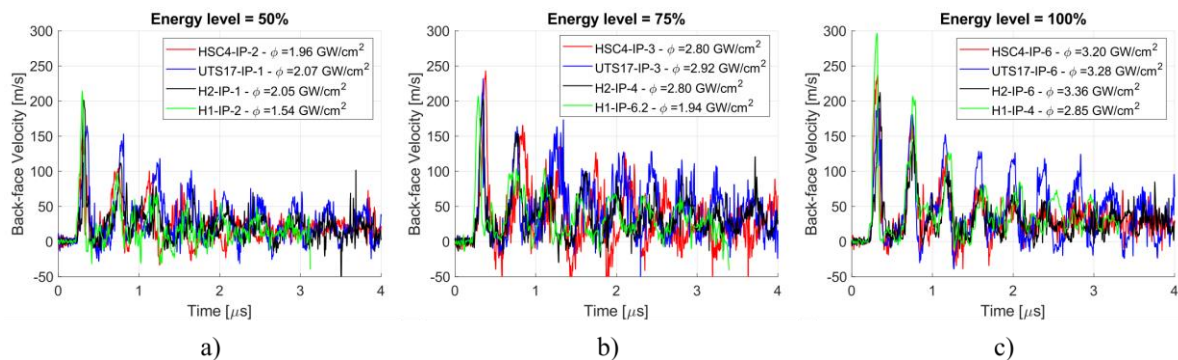


Fig. 4.4. Back-face velocity versus time comparison for all laminates, for different energy levels; a) 50%; b) 75%; c) 100%

#### 4.7.1.2 Hugoniot Elastic Limit

The prior arrival of the elastic wave is seen in most in-plane samples as a small step below 50 m/s in the back-face velocity signal, ahead of the main shock front, and it represents the Hugoniot Elastic Limit (HEL). Considering the velocity of the HEL at  $\sim 30$  m/s, and a propagation speed of  $\sim 10$  km/s, the HEL limit would be 222 MPa. In the fiber direction, Alexander et al. [96] determined a HEL limit of 3.5 GPa for unidirectional carbon fiber composites, which is significantly higher than the value obtained from the in-plane laser tests. Smith et al. [97] identified the HEL on the back-face velocity trace from laser-induced shockwaves test on aluminum samples at approximately 25 m/s, giving a HEL limit of 176 MPa, much closer to the one estimated here. Therefore, it is concluded that the discontinuity in the rising front of the back-face velocity, in the case of laser-induced shockwave tests in the fiber direction of the studied composite represents the HEL of the aluminum sacrificial layer and not the HEL of the carbon fiber composite.

#### 4.7.1.3 Speed of sound estimation from in-plane Laser-induced shockwave tests

The propagation period was extracted through FFT analysis, and the speed of sound was evaluated between 10 km/s and 11 km/s, depending on the laminate type, with UTS laminates having the highest speed of sound in the fiber direction. By comparing the theoretical longitudinal speed of sound with experimental data, it was observed that by using the properties of the carbon fiber when estimating the longitudinal speed of sound rather than the laminate quasi-static properties, closer results are obtained. This is another confirmation that with the in-plane laser impact tests, the response of the fibers is mainly captured.

#### 4.7.1.4 Damage analysis

Even though the back-face velocity signals showed only spallation of the gold particles, the samples shot at 75% and 100% of max energy showed visible signs of damage, but not in the form of a spall but as matrix cracking and fiber breakage. Besides the principal matrix crack, other thin lines of matrix crack propagation could be observed for all inspected samples shot with an energy level above 75%, as seen in Fig. 4.5. As microscopic observations were performed in the rupture plane of one of the H1 samples, it was observed that part of the fibers were broken, most of them closer to the back face. Also broken fiber bundles could be identified. Although some fibers were broken, there was not a clear fracture plane for all of them, which is probably why a clear spall signal could not be obtained for the back face velocity.

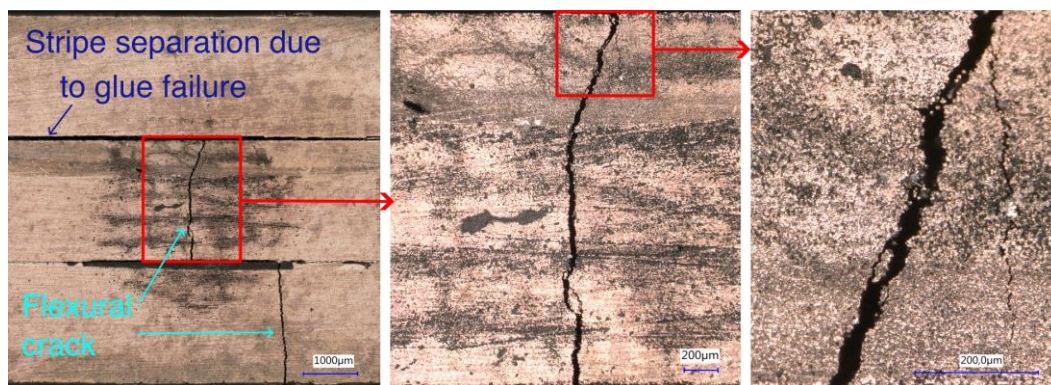


Fig. 4.5 Visible damage on the back-face of H1-IP-1 sample, shot at 100% of max energy level with  $\phi=2.30$  GW/cm<sup>2</sup>

Based on microscopic observations of matrix cracks visible on the back face and the laser shot's density of power (excluding stripe separation), a matrix failure threshold for the in-fiber direction laser shots for all tested materials was established. For UTS and HSC laminates, the matrix failure threshold is  $\sim 2.8$  GW/cm<sup>2</sup>, while for the hybrid laminates, the gap between the damaged and undamaged samples is wider. For H1, the matrix failure threshold is in the density

of power interval of 2 – 2.8 GW/cm<sup>2</sup>, while for H1 the matrix failure threshold is lower, at a density of power between 1.4 and 1.9 GW/cm<sup>2</sup>.

#### 4.7.2 Out-of-plane laser-induced shockwave test results

##### 4.7.2.1 Back-face velocity signal analysis for out-of-plane laser tests

By analyzing the back-face velocity signals for the out-of-plane laser impact tests (i.e., the direction of the shock propagation is normal to the ply plane), it was observed that the first peak has a lower amplitude with decreasing energy level and density of power of the laser shot, as seen in Fig. 4.6. Moreover, laser shots at high energy levels exhibited a spall signal. When evaluating the sample thickness effects on the back-face velocity trace, it was observed that the increased thickness leads to a delay in the shock arrival, and a decrease in the maximum velocity of the first peak, caused by shockwave attenuation.

A linear decreasing trendline of the maximum back-face velocity with the thickness of the sample is apparent. Additionally, the type of carbon fiber composite does not exert any significant influence on the maximum back-face velocity within the range of tested thicknesses.

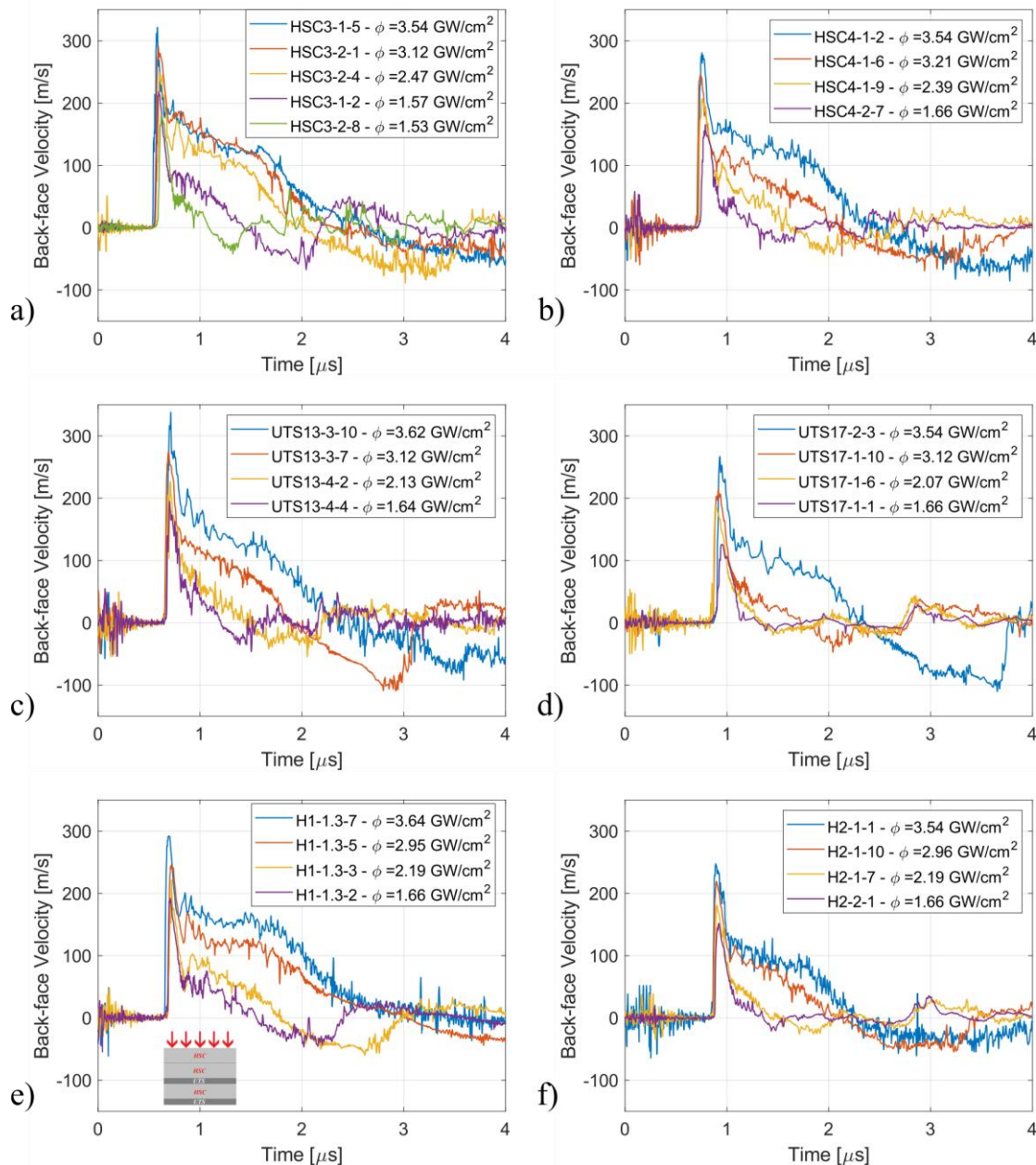


Fig. 4.6. Representative back-face velocity versus time signals for all tested materials, at different energy levels, with the corresponding density of power; a) HSC3; b) HSC4; c) UTS13; d) UTS17; e) H1 (2022 experimental campaign); f) H2

As the H1 composite has an unsymmetric stacking sequence, the influence of impacting the sample on one face or the other is studied. In this regard, pairs of samples with opposite stacking sequences were tested in both the 2021 and 2022 experimental campaigns. At lower densities of power, the difference between samples impacted on the HSC or UTS ply is negligible. As the density of power increases, the difference in the velocities' values also increases for the samples tested in the 2021 campaign. However, when incorporating the peak velocities from the 2022 campaign, the previously observed difference in the peak velocity is not present anymore. When examining the 100% and 75% of max energy shots for samples impacted on the UTS ply, the spall signal does not display a clear mean velocity before starting to decrease, in contrast to shots on samples impacted on the HSC ply. Furthermore, the mean spall velocity for samples tested in the 2021 campaign is not as distinct as those tested in 2022, particularly at higher intensities. These findings suggest that for H1 samples impacted on the HSC face, a clear plane rupture should exist, while for samples impacted on the UTS ply, the rupture plane might be irregular.

#### 4.7.2.2 *Parameters estimation from Laser-induced shockwave tests*

The sound speed in the out-of-plane direction was evaluated by measuring the time difference between the first and second shockwave breakout for shots that did not produce any damage in the composites, giving average values between 2.75 km/s and 2.91 km/s, with no significant differences between the reference laminates. The dynamic tensile strength was evaluated from shots that exhibited a clear spall signal according to Novikov approach [82] and was estimated between 289 MPa and 317 MPa, with average strain rates during spall fracture between  $1.75 \times 10^5 \text{ s}^{-1}$  and  $1.91 \times 10^5 \text{ s}^{-1}$ .

#### 4.7.2.3 *Damage analysis*

Through microscopic observation of cross-sections close to the centerline of the laser impact focal spot, part of the samples that presented a spall signal were further analyzed to confirm the presence of damage within the samples. Although a delamination between plies was expected in most cases, for all laminates except for H1 impacted on the HSC face, damage was in the form of intraply matrix crack, thus a spallation. Examples are given in in Fig. 4.7 for HSC3 samples. UTS laminates exhibited spallation in the second to last ply, while HSC samples and hybrid laminates showed damage in the last HSC ply. Damage was mostly located at similar positions relative to the back-face, at around 250  $\mu\text{m}$ . For H1 impacted on the HSC face, damage was in the form of delamination between the last HSC and UTS plies. It was more regular, visible and extended compared to the spallation observed in the case of H1 samples impacted on the UTS face.

Damage thresholds were established for each material, and UTS laminates prove to have the highest damage threshold and the threshold is also influenced by sample thickness.

Damage assessments reveal that short duration, high-energy loading can lead to substantial damage within the composite sample. This damage often manifests as barely visible impact-related issues that are challenging to detect with the naked eye. Furthermore, such damage has the potential to compromise the structural integrity of the material.

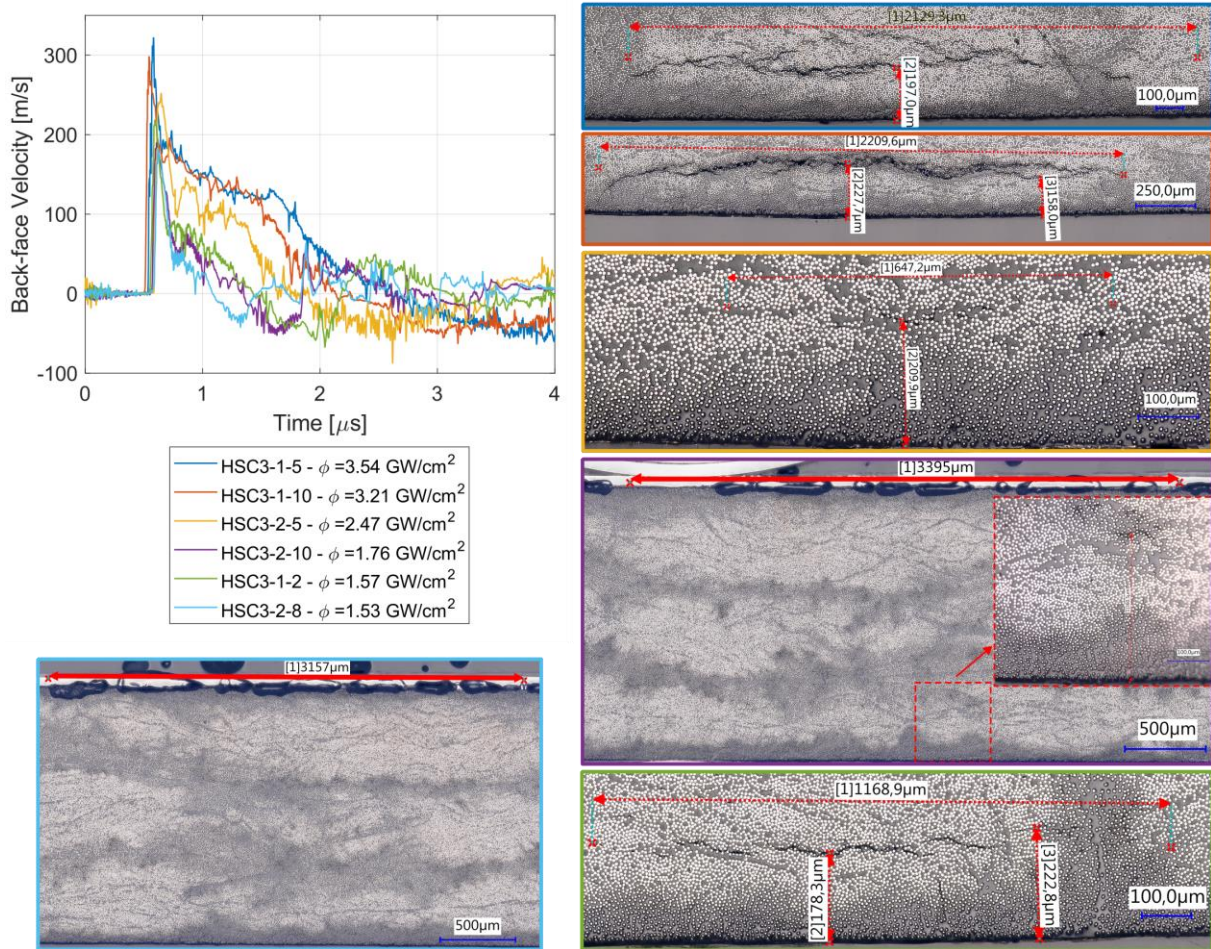


Fig. 4.7. Microscopic observations of damage induced by laser impact in HSC3 samples, cutting plane perpendicular to the fiber direction, with corresponding back-face velocity signals

## PART 2: STEEL BALL IMPACT

### 4.8 SAMPLE DESCRIPTION AND EXPERIMENTAL SETUP

To conduct the steel ball impact test, four flat panels measuring 250 × 210 mm (fiber direction on the long edge) were cut from a 500 × 500 mm composite panel. The ply-level hybrid material used for this test is H2, with a stacking sequence of HSC+UTS+2HSC+UTS+HSC [0°] (see Fig. 2.1). Rectangular aluminum end-tabs measuring 210 × 25 mm with a thickness of 1.5 mm were glued using Araldite 420 A/B Epoxy Adhesive System. The samples were securely held in place by a clamping system situated at both the top and bottom of the sample.

For this test, a single stage Taylor gun was used, with a maximum pressure of 20bar in the air tank. A stainless-steel ball (AISI 316) with a diameter of 10 mm and a mass of 4.171 g served as the projectile. This steel ball was positioned within a sabot and inserted into the gun's barrel. To gauge the speed of the sabot, two photodiodes were placed 7.3 cm apart near the barrel's end. In an effort to ascertain the ball's velocity both before and after impact, a high-speed Photron Fastcam SA-X2 camera was employed. The captured images were subsequently subjected to post-processing.

### 4.9 STEEL BALL IMPACT EXPERIMENTAL RESULTS

For the first shot, with a velocity before impact of 170m/s, the ball passed through the composite causing damage in the sample in form of stripes with an approximate width of 3mm that reached the end-tabs. For the second shot, a lower pressure was used to avoid damage reaching the end-tabs. The ball had an impact velocity of 107m/s and rebounded. Only matrix cracks along the fibers were observed, close to the end-tabs but without reaching them. For the

next two shots, with even lower pressures and corresponding impact velocities of 56m/s and 39m/s, no apparent damage was observed, with the exception of the mark left by the ball at the impact point. The steel ball impact test was intended as a structural test for further numerical simulation validation and showed that H2 material absorbs almost 90% of the incident kinetic energy, for all impact velocities tested.

#### SUMMARY

Through the analysis performed in this chapter, insight on the behavior of unidirectional carbon fiber composite materials under dynamic loading conditions, at high and very high strain rates was obtained, attaining objectives 5, 6 and 7. Laser-induced shockwaves tests in the fiber direction and in the out-of-plane direction were performed to analyze the composite behavior under very high strain rate loading as well as to evaluate damage, spallation and delamination within the composite, caused by shock propagation. Steel ball impact tests on H2 material were also performed, to address damage caused by foreign object impact at velocities below the ballistic regime ( $<200$  m/s), as well as the absorbed energy by the composite plate.

## CONCLUSIONS, CONTRIBUTIONS, AND OUTLOOKS

### CONCLUSIONS

The research work presented in this thesis contributes to the understanding of the mechanical behavior of unidirectional composite materials, and also introduces the concept of ply-level hybridization in both ply thickness and carbon fiber type, addressing the effects of such a hybridization as well. Referring back to the objectives of the thesis, mentioned in the Introduction section, the following aspects were addressed:

1. The experimental characterization of internal structure and physical properties of reference and ply-level hybrid unidirectional carbon composite materials
2. Evaluation of the quasi-static mechanical response of hybrid and reference laminates under on and off-axis tensile testing;
3. The cause of the nonlinear off-axis response, through off-axis cyclic load-unload tensile tests and the evaluation of residual strains and damage variables;
4. The definition of a coupled damage-plasticity model for predicting the nonlinear off-axis response of laminates
5. Evaluation of the shockwave propagation in the reference and ply-level hybrid materials, in the fiber direction and perpendicular to the fiber direction
6. Delamination and spall fracture at high-strain rates, and evaluation of dynamic tensile strength
7. Damage position and threshold evaluation for the different configurations of the studied composites

The objectives were attained, along with the primary aim of the study, and the following general conclusions can be drawn. In order to address the first objective, a comprehensive analysis of the properties of the studied materials was performed in Chapter 2, involving the measurement of density using two approaches - mass and dimensions measurements, and by Archimedes principle; measurements of fiber volume fraction by burn-off procedure; void content estimation by 2D microscopy and areal fraction measurements; internal structure analysis and identification of internal defects. Density measurements conducted through Archimedes' principle were deemed to be more reliable. This choice was driven by the understanding that slight irregularities in the flatness of the edges introduced measurement errors when using dimensional methods, impacting the accuracy of the overall density estimation. The studied composites exhibit similar densities with differences of up to 1.42%. The burn-off method for fiber volume content estimation proved to be suitable and safe for the tested carbon-fiber composites, with no resin residue visible on the fibers after a complete burn-off cycle. The fiber volume fraction was estimated between 49% and 54%, with HSC laminates having the lowest fiber content. Considering the prepregs datasheet, this outcome was expected. The microscopic observation of the laminates' cross-sections revealed that UTS composites, having thinner prepreg plies, display a more uniform distribution of the fibers, reduced ply-waviness, with a ply interface that is not rich in resin and easily identifiable. However, they exhibited a higher percentage of interply voids. The laminates with thicker HSC plies exhibited ply mixing, rich-resin regions, and ply waviness, along with intraply voids. The internal structure analysis of the hybrid laminates indicated improvements in terms of ply mixing, resin-

rich regions, and ply waviness when compared with HSC laminates. In all studied laminates, the estimated void content falls below 1%, suggesting that the mechanical properties of these composites should not be affected by the void content.

Moving forward to analyzing the mechanical response of the composites of interest, and addressing objectives 2, and 3, quasi-static tensile tests were performed in the fiber direction, perpendicular to the fiber direction, and at three off-axis angles: 15°, 30°, and 45°. For damage assessment and evaluation of parameters required for the definition of a coupled damage-plasticity model in order to predict the nonlinear behavior of unidirectional laminates loaded off-axis, quasi-static cyclic load-unload tests were performed for the same three off-axis angles. The results, presented in Chapter 3, show no significant thickness effects on the stress-strain response under both longitudinal and transverse quasi-static tensile loading. For equivalent thickness and sample geometry, hybrid composites exhibited an improved 0° failure stress compared to the estimated strength based on Kawai's scaling function.

For the transverse failure stress, high dispersion of data was obtained because most samples failed close to the grips, and the results presented high error bars. Off-axis tests exhibited nonlinear behavior with the degree of nonlinearity decreasing with increasing off-axis angles. Minor differences were found in the linear response region, but HSC laminates showed strain hardening in the nonlinear region, albeit with smaller failure strain than UTS laminates.

Hybrid laminates displayed higher failure stress and intermediate failure strains compared to simple laminates, also exhibiting a strain hardening compared to reference laminates. Laminate thickness did not significantly affect stress-strain responses in the linear region, but slight differences emerged in the nonlinear region for laminates of the same material but with different thicknesses. The experimental data aligned with predictions using theoretical equations, indicating off-axis elastic moduli and strength degradation with increasing off-axis angles.

In general, the hybridization approach demonstrated significant advantages, such as improved strain-hardening behavior and increased failure stress compared to the reference laminates. Furthermore, the behavior of hybrid laminates resembled that of a transversely isotropic system.

The cyclic load-unload tests revealed that the nonlinearity of off-axis response results from a combination of internal damage and residual strain. Damage variable evolution and accumulated residual strain were quantified by studying incremental loading/unloading stress-strain responses. Overall, UTS laminates exhibited the highest residual strains, suggesting the UTS matrix prepreg's inherent plasticity compared to HSC laminates. Hybrid laminates, on the other hand, exhibited lower residual strains across all scenarios. Three methods - Ladeveze, Fitoussi, and Regression - were used to estimate the damage variable. Regression proved unreliable due to irregular damage variable changes with increasing stress levels, yielding negative values and high error margins.

To fulfill objective 4 and define a nonlinear constitutive model for predicting off-axis behavior in unidirectional ply-level hybrid composites, parameters were derived from experimental data on residual strain and damage variables. Only damage variables obtained through Ladeveze and Fitoussi methods were considered for predicting off-axis behavior. These predictions generally matched experimental results in the linear response region and satisfactory results were obtained in the nonlinear response region. Furthermore, damage and plasticity parameters from thinner laminates of the same material prepregs were used to predict responses in thicker reference laminates, yielding improved results for UTS17 and satisfactory outcomes for HSC4. Predictions for hybrid laminates' off-axis responses, using damage parameters from hybrid laminates and plasticity parameters from HSC laminates, showed significant improvements in the nonlinear response region. This underscores the importance of plasticity parameters and suggests that matrix plasticity in HSC plies primarily governs the softening observed in the nonlinear response region of tested hybrid laminates.

Forwarding to more complex loadings, the mechanical response under very-high strain rate loading was analyzed using laser-induced shockwave tests (Chapter 4), to address objectives 5, 6, and 7. The propagation of shockwaves in the reference and hybrid laminates, in both longitudinal and transverse directions, was evaluated by employing back-face velocity analysis.

Laser impact tests were conducted in the fiber direction (in-plane) at three energy levels. Analysis of the back-face velocity signal, recorded through laser-Doppler interferometry, revealed a decrease in the maximum velocity of the first peak with decreasing energy level. Spallation of the gold layer on the back-face, used for enhanced reflectivity, was observed in two H1 samples and slightly affected the back-face velocity signal extraction.

The propagation period was determined through FFT analysis, yielding sound speeds between 10 km/s and 11 km/s, dependent on the laminate type, with UTS laminates exhibiting the highest speed of sound in the fiber direction. A comparison of the theoretical longitudinal speed of sound with experimental data indicated that using carbon fiber properties for estimating longitudinal sound speed provided more accurate results than using laminate quasi-static properties.

While the back-face velocity signals showed spallation of gold particles, samples subjected to 75% and 100% of max energy levels exhibited visible damage, including intralaminar matrix cracking and fiber breakage, rather than spallation. Microscopic examination revealed broken fibers, primarily closer to the back face, and broken fiber bundles. The lack of a clear fracture plane for all fibers likely contributed to the absence of a distinct spall signal.

For out-of-plane laser impact tests (shock propagation normal to the ply plane), two experimental campaigns were conducted, one in 2021 and the other in 2022. It was observed that the first peak in the back-face velocity signal had a lower amplitude with decreasing energy level and laser power density. High-energy laser shots produced spallation.

Sample thickness influenced the back-face velocity trace, with increased thickness causing delayed shock arrival and reduced maximum first peak velocity due to shockwave attenuation. The impact on either the UTS or HSC face of H1 material was compared. For tests performed in 2021, shots on the UTS face exhibited higher maximum first peak velocities, but this difference was not significant for tests performed in 2022.

Sound speed in the out-of-plane direction was evaluated by measuring the time difference between the first and second shockwave breakout for shots without composite damage, yielding average values between 2.75 km/s and 2.91 km/s, with no significant differences among reference laminates and hybrid ones. Dynamic tensile strength, determined using the Novikov approach from shots with clear spall signals, ranged between 289 MPa and 317 MPa, with close results between the reference and hybrid laminates.

Microscopic analysis of cross-sections near the center of the laser impact focal spot was performed on samples that exhibited spall signals. Contrary to the expected delamination between plies, all laminates except H1 impacted on the HSC face showed intraply matrix cracks, resembling spallation. UTS laminates had spallation in the second-to-last ply, while HSC samples and hybrid laminates had damage in the last HSC ply, typically around 250  $\mu\text{m}$  from the back face. In the case of H1 impacted on the HSC face, delamination occurred between the last HSC and UTS plies, appearing more regular, visible, and extensive compared to spallation observed when impacted on the UTS face. Damage thresholds were determined for each material, with UTS laminates having the highest damage threshold, which was also influenced by sample thickness.

The assessments revealed that short-duration, high-energy loading could result in significant damage within the composite sample. This damage often presents as nearly imperceptible impact-related issues that are challenging to discern with the naked eye. Furthermore, such damage has the potential to compromise the structural integrity of the material, revealing the necessity for a better understanding of the phenomenon.

Additionally, steel ball impact tests were performed on H2 samples, to evaluate the energy absorption capacity of the unidirectional composite laminate and damage mechanism during

high-velocity impact loading with a foreign object. Four tests at different pressures in the Taylor gun were performed. In the first test, at maximum pressure, the steel ball penetrated the laminate plate. However, the induced damage in the laminate was constrained by the end-tabs, deeming the test unreliable for damage assessments. For subsequent tests, lower pressures were used to prevent damage from reaching the end-tabs. In these cases, the steel ball rebounded. No additional testing was performed for the other laminate configurations in this thesis, as the unidirectional laminate proved to be unsuitable for this type of test, requiring larger sample dimensions to avoid end-tab effects. However, these first results remain a set of experimental results to be matched with numerical modelling.

## CONTRIBUTIONS

Considering the aim and objectives of this thesis, the following original contributions are highlighted:

1. Introduction of a novel approach to ply-level hybridization, by considering carbon fibers with different quality besides the different ply thickness, for cost reduction purposes;
2. Implementing a successive linear regression procedure, to determine the linear response region of nonlinear off-axis response, to determine the apparent Young modulus and Poisson ratio;
3. Use and comparison of three distinctive methods of evaluating the damage variable from cyclic load-unload tensile testing, and their effects on prediction models;
4. Use of damage and plasticity parameters from thinner laminates to predict the nonlinear behavior of thicker laminates of the same prepreg type;
5. Experimental testing using laser-induced shockwaves in the fiber direction, considering a new method of obtaining a viable testing sample from thin unidirectional laminates;
6. Analysis of laser impact on opposite faces of laminates with asymmetric stacking sequence;
7. Synthesis of the experimental campaigns and analysis of the all-carbon ply-level hybridization effects on the mechanical response of carbon fiber composites under quasi-static and high-strain rate dynamic loading.

## OUTLOOKS

The work in this thesis leads to interesting perspectives from which the following are of notable interest.

As the coupled damage-plasticity model employed in Chapter 3 proved to be able to predict the nonlinear off-axis behavior of the composites with satisfactory error margins, another point would be to extend the analytical damage-plasticity model and include it in a numerical model, for more accurate predictions and structure optimization. By calibrating the numerical model using the experimental data from this work, additional laminate configurations can be explored, to optimize and tailor the hybrid composite response to specific applications,

The novel back-face velocity traces in the fiber direction from this thesis lack a spall trace even at the highest energy levels available in the testing facility. However, in one sample microscopic observations could be performed and broken fibers were observed. It would be of interest to manufacture thick unidirectional samples and test them at even higher energy values and densities of power, to assess if spallation can be obtained in purely unidirectional composites.

Moreover, the issue of damage detection is a critical aspect. This study demonstrates that measuring the back-face velocity provides significant insight. It facilitates an accurate description of phenomena and effectively distinguishes between damage and non-damage events. Moreover, for the first time, it was observed that laser-induced shockwaves can produce spallation inside the composite ply, and not only delamination at the ply interface. However, in terms of quantifying internal damage, the destructive microscopic cross-section analysis is section-biased, limited to one direction, and also prone to off-center positioning due to sensitive

sample preparation. Although not available in this study, micro-tomography observation using a sufficiently high resolution could be a valuable addition to understanding spallation propagation in unidirectional composites.

Considering that damage caused by laser-induced shockwaves is internal and in the form of barely visible impact damage which is difficult to observe, for structural applications, it would be of interest to assess the mechanical properties of the laminate after such an impact, for example, the compression after impact strength.

Although not addressed in this work, numerical modeling of the laser impact, both in the fiber and in the out-of-plane direction, calibrated using the experimental data in this work, would provide valuable information and additional insight on shockwave propagation inside the laminates, the effects of fiber orientation, and additional hybridization effects on the propagation of the shockwaves. When testing the H1 samples on opposite stacking sequences, different back-face velocity amplitudes were observed between the configurations in one experimental campaign. However, in the second experimental campaign, the differences were not present. For now, this phenomenon is yet to be explained, and numerical simulations could provide valuable in understanding the underlying causes for the observed phenomenon.

## PUBLICATIONS

Part of this thesis work was published in scientific journals and presented at scientific conferences. The author led the following publications:

### Journal publications:

- **M. Casapu**, I. Fuiorea, and M. Arrigoni, *Experimental Characterization of Internal Structure and Physical Properties of Unidirectional Ply-Level Hybrid Carbon Composite Material*, *Advanced Engineering Materials*, 2023, DOI: 10.1002/ADEM.202201447.
- **M. Casapu**, M. Arrigoni, and I. Fuiorea, *Off-axis response and shear characterization of unidirectional ply-level hybrid carbon-fiber-reinforced polymer materials*, *INCAS BULLETIN*, vol. 15, no. 3, pp. 31–46, 2023, DOI: 10.13111/2066-8201.2023.15.3.3.
- **M. Casapu**, I. Fuiorea, and M. Arrigoni, *Damage assessment through cyclic load-unload tensile tests for ply-level hybrid carbon fiber composites*, *Express Polymer Letters*, vol. 18, no. 1, pp. 41-60, 2024, DOI: 10.3144/expresspolymlett.2024.4.
- **M. Casapu**, A. C. Casapu, M. Arrigoni, and I. Fuiorea, *Laser-induced Shockwaves for Damage Assessment and Characterization at High Strain Rates in the Fiber Direction of Unidirectional Composites*, *Materials Letters - (Revision pending)*.

### Conference presentations:

- **M. Casapu**, I. Fuiorea, and M. Arrigoni, *Experimental Characterization of Internal Structure and Physical Properties of Unidirectional Ply-Level Hybrid Carbon Composite Material*, 15th International Conference on Advanced Computational Engineering and Experimenting – ACEX2022, Florence, Italy, 2022.
- **M. Casapu**, A. C. Casapu, M. Arrigoni, and I. Fuiorea, *Laser-induced Shockwaves for Damage Assessment and Characterization at High Strain Rates in the Fiber Direction of Unidirectional Composites*, 27<sup>th</sup> DYMAT Technical Meeting, Colmar, France, 2023.

## SELECTIVE BIBLIOGRAPHY

- [1] International Civil Aviation Organization, 2021 global air passenger totals show improvement from 2020, but still only half pre-pandemic levels. <https://www.icao.int/Newsroom/Pages/2021-global-air-passenger-totals-show-improvement.aspx> (accessed Jul. 26, 2022).
- [2] C. Soutis, Carbon fiber reinforced plastics in aircraft construction, *Materials Science and Engineering: A*, vol. 412, no. 1–2, pp. 171–176, 2005, doi: 10.1016/J.MSEA.2005.08.064.
- [3] D. Gay, *Composite materials : design and applications*, Third Edit. Boca Raton: CRC Press, 2015.
- [4] T. Jollivet, C. Peyrac, and F. Lefebvre, Damage of composite materials, *Procedia Engineering*, vol. 66, pp. 746–758, 2013, doi: 10.1016/j.proeng.2013.12.128.
- [5] I. M. Daniel and O. Ishai, *Engineering mechanics of composite materials*. Oxford University Press, 1994.
- [6] A. Rajpurohit, S. Joannès, V. Singery, P. Sanial, and L. Laiarinandrasana, Hybrid Effect in In-Plane Loading of Carbon/Glass Fibre Based Inter- and Intraply Hybrid Composites, *Journal of Composites Science 2020, Vol. 4, Page 6*, vol. 4, no. 1, p. 6, 2020, doi: 10.3390/JCS4010006.
- [7] E. Randjbaran, R. Zahari, A. A. N. Jalil, and D. L. A. A. Majid, Hybrid Composite Laminates Reinforced with Kevlar/Carbon/Glass Woven Fabrics for Ballistic Impact Testing, 2014, doi: 10.1155/2014/413753.
- [8] A. R. Bunsell and B. Harris, Hybrid carbon and glass fibre composites, *Composites*, vol. 5, no. 4, pp. 157–164, 1974, doi: 10.1016/0010-4361(74)90107-4.
- [9] G. Czél and M. R. Wisnom, Demonstration of pseudo-ductility in high performance glass/epoxy composites by hybridisation with thin-ply carbon prepreg, *Composites Part A: Applied Science and Manufacturing*, vol. 52, pp. 23–30, 2013, doi: 10.1016/J.COMPOSITESA.2013.04.006.
- [10] G. Czél, M. Jalalvand, and M. R. Wisnom, Demonstration of pseudo-ductility in unidirectional hybrid composites made of discontinuous carbon/epoxy and continuous glass/epoxy plies, *Composites Part A: Applied Science and Manufacturing*, vol. 72, pp. 75–84, 2015, doi: 10.1016/J.COMPOSITESA.2015.01.019.
- [11] A. Arteiro, C. Furtado, G. Catalanotti, P. Linde, and P. P. Camanho, Thin-ply polymer composite materials: A review, *Composites Part A: Applied Science and Manufacturing*, vol. 132, p. 105777, 2020, doi: 10.1016/J.COMPOSITESA.2020.105777.
- [12] S. Sihm, R. Y. Kim, K. Kawabe, and S. W. Tsai, Experimental studies of thin-ply laminated composites, *Composites Science and Technology*, vol. 67, no. 6, pp. 996–1008, 2007, doi: 10.1016/J.COMPSCITECH.2006.06.008.

- [13] L. C. Alil, M. Arrigoni, M. Istrate, A. Kravcov, J. Le Pavic, and G. Tahan, Laser Induced Shockwave as Delaminator of Composite Material for Ballistic Protection at High Strain Rate, *NATO Science for Peace and Security Series C: Environmental Security*, pp. 15–33, 2020, doi: 10.1007/978-94-024-1755-5\_2.
- [14] S. Ekşi and K. Genel, Comparison of Mechanical Properties of Unidirectional and Woven Carbon, Glass and Aramid Fiber Reinforced Epoxy Composites, *Acta Physica Polonica Series A*, vol. 132, no. 3–II, pp. 879–882, 2017, doi: 10.12693/APhysPolA.132.879.
- [15] G. Marsh, Prepregs — raw material for high-performance composites, *Reinforced Plastics*, vol. 46, no. 10, pp. 24–28, 2002, doi: 10.1016/S0034-3617(02)80172-2.
- [16] Y. Chen, J. Zhang, Z. Li, H. Zhang, J. Chen, W. Yang, T. Yu, W. Liu, and Y. Li, Manufacturing Technology of Lightweight Fiber-Reinforced Composite Structures in Aerospace: Current Situation and toward Intellectualization, *Aerospace 2023, Vol. 10, Page 206*, vol. 10, no. 3, p. 206, 2023, doi: 10.3390/AEROSPACE10030206.
- [17] C. Soutis, Fibre reinforced composites in aircraft construction, *Progress in Aerospace Sciences*, vol. 41, no. 2, pp. 143–151, 2005, doi: 10.1016/J.PAEROSCI.2005.02.004.
- [18] M. V. Ramana and S. Ramprasad, Experimental Investigation on Jute/Carbon Fibre reinforced Epoxy based Hybrid Composites, *Materials Today: Proceedings*, vol. 4, no. 8, pp. 8654–8664, 2017, doi: 10.1016/J.MATPR.2017.07.214.
- [19] L. Ferrante, J. Tirillò, F. Sarasini, F. Touchard, R. Ecault, M. A. Vidal Urriza, L. Chocinski-Arnault, and D. Mellier, Behaviour of woven hybrid basalt-carbon/epoxy composites subjected to laser shock wave testing: Preliminary results, *Composites Part B: Engineering*, vol. 78, pp. 162–173, 2015, doi: 10.1016/j.compositesb.2015.03.084.
- [20] J. H. Song, Pairing effect and tensile properties of laminated high-performance hybrid composites prepared using carbon/glass and carbon/aramid fibers, *Composites Part B: Engineering*, vol. 79, pp. 61–66, 2015, doi: 10.1016/J.COMPOSITESB.2015.04.015.
- [21] D. W. Lee, B. J. Park, S. Y. Park, C. H. Choi, and J. Il Song, Fabrication of high-stiffness fiber-metal laminates and study of their behavior under low-velocity impact loadings, *Composite Structures*, vol. 189, pp. 61–69, 2018, doi: 10.1016/j.compstruct.2018.01.044.
- [22] K. Dadej, J. Bienias, and B. Surowska, On the effect of glass and carbon fiber hybridization in fiber metal laminates: Analytical, numerical and experimental investigation, *Composite Structures*, vol. 220, pp. 250–260, 2019, doi: 10.1016/J.COMPSTRUCT.2019.03.051.
- [23] P. T. Curtis and M. Browne, Cost-effective high performance composites, *Composites*, vol. 25, no. 4, pp. 273–280, 1994, doi: 10.1016/0010-4361(94)90219-4.
- [24] K. Naito, J. M. Yang, and Y. Kagawa, Tensile properties of high strength polyacrylonitrile (PAN)-based and high modulus pitch-based hybrid carbon fibers-reinforced epoxy matrix composite, *Journal of Materials Science*, vol. 47, no. 6, pp. 2743–2751, 2012, doi: 10.1007/S10853-011-6101-8.
- [25] G. Czél, M. Jalalvand, M. R. Wisnom, and T. Czigány, Design and characterisation of high performance, pseudo-ductile all-carbon/epoxy unidirectional hybrid composites, *Composites Part B: Engineering*, vol. 111, pp. 348–356, 2017, doi: 10.1016/J.COMPOSITESB.2016.11.049.
- [26] C. Furtado, A. Arteiro, G. Catalanotti, J. Xavier, and P. P. Camanho, Selective ply-level hybridisation for improved notched response of composite laminates, *Composite Structures*, vol. 145, pp. 1–14, 2016, doi: 10.1016/J.COMPSTRUCT.2016.02.050.
- [27] S. Abrate, *Impact engineering of composite structures*. Springer, 2011.
- [28] M. R. Wisnom, The role of delamination in failure of fibre-reinforced composites,

- Philosophical Transactions of the Royal Society A: Mathematical, Physical and Engineering Sciences*, vol. 370, no. 1965, pp. 1850–1870, 2012, doi: 10.1098/rsta.2011.0441.
- [29] T. W. Shyr and Y. H. Pan, Impact resistance and damage characteristics of composite laminates, *Composite Structures*, vol. 62, no. 2, pp. 193–203, 2003, doi: 10.1016/S0263-8223(03)00114-4.
- [30] N. K. Naik and P. Shirao, Composite structures under ballistic impact, *Composite Structures*, vol. 66, no. 1–4, pp. 579–590, 2004, doi: 10.1016/j.compstruct.2004.05.006.
- [31] V. V. Silberschmidt, *Dynamic deformation, damage and fracture in composite materials and structures*, 1st ed. Elsevier Ltd, 2016.
- [32] ASTM International, ASTM D3039/D3039M - Standard Test Method for Tensile Properties of Polymer Matrix Composite Materials, 2000
- [33] British Standards Institution, BS EN ISO 527-5:2009: Plastics. Determination of tensile properties. Test conditions for unidirectional fibre-reinforced plastic composites, 2009
- [34] M. R. Wisnom, B. Khan, and S. R. Hallett, Size effects in unnotched tensile strength of unidirectional and quasi-isotropic carbon/epoxy composites, *Composite Structures*, vol. 84, no. 1, pp. 21–28, 2008, doi: 10.1016/J.COMPSTRUCT.2007.06.002.
- [35] M. Kawai, K. Watanabe, H. Hoshi, E. Hara, and Y. Iwahori, Effect of specimen size on longitudinal strength of unidirectional carbon/epoxy composite laminates (part 1, unnotched strength), *Advanced Composite Materials*, vol. 28, pp. 53–71, 2019, doi: 10.1080/09243046.2018.1458269.
- [36] R. M. Jones, *Mechanics Of Composite Materials*, 2nd ed. New York: Taylor & Francis, 1999. doi: 10.1201/9781498711067.
- [37] M. J. Pindera and C. T. Herakovich, Shear characterization of unidirectional composites with the off-axis tension test, *Experimental Mechanics*, vol. 26, no. 1, pp. 103–112, 1986, doi: 10.1007/BF02319962.
- [38] M. J. Pindera, G. Choksi, J. S. Hidde, and C. T. Herakovich, A Methodology for Accurate Shear Characterization of Unidirectional Composites, *Journal of Composite Materials*, vol. 21, no. 12, pp. 1164–1184, 1987, doi: 10.1177/002199838702101205.
- [39] C. C. Chamis and J. H. Sinclair, Ten-deg Off-axis Test for Shear Properties in Fiber Composites, *Experimental Mechanics*, vol. 17, pp. 339–346, 1977.
- [40] G. Vargas and F. Mujika, Determination of In-plane Shear Strength of Unidirectional Composite Materials Using the Off-axis Three-point Flexure and Off-axis Tensile Tests, *Journal of Composite Materials*, vol. 44, no. 21, pp. 2487–2507, 2010, doi: 10.1177/0021998310369601.
- [41] M. M. Shokrieh and M. J. Omid, Investigation of strain rate effects on in-plane shear properties of glass/epoxy composites, *Composite Structures*, vol. 91, no. 1, pp. 95–102, 2009, doi: 10.1016/J.COMPSTRUCT.2009.04.035.
- [42] H. Koerber, J. Xavier, and P. P. Camanho, High strain rate characterisation of unidirectional carbon-epoxy IM7-8552 in transverse compression and in-plane shear using digital image correlation, *Mechanics of Materials*, vol. 42, no. 11, pp. 1004–1019, 2010, doi: 10.1016/j.mechmat.2010.09.003.
- [43] Y. Liang, H. Wang, and X. Gu, In-plane shear response of unidirectional fiber reinforced and fabric reinforced carbon/epoxy composites, *Polymer Testing*, vol. 32, no. 3, pp. 594–601, 2013, doi: 10.1016/j.polymertesting.2013.01.015.
- [44] A. K. Ditcher, F. E. Rhodes, and J. P. H. Webber, Non-Linear Stress-Strain Behaviour Of

- Carbon Fibre Reinforced Plastic Laminates, *Journal of Strain Analysis*, vol. 16, no. 1, pp. 43–51, 1981, doi: 10.1243/03093247V161043.
- [45] C. T. Sun and J. L. Chen, A Simple Flow Rule for Characterizing Nonlinear Behavior of Fiber Composites, *Journal of Composite Materials*, vol. 23, no. 10, pp. 1009–1020, 1989, doi: 10.1177/002199838902301004.
- [46] J. Cho, J. Fenner, B. Werner, and I. M. Daniel, A Constitutive Model for Fiber-reinforced Polymer Composites, *Journal of Composite Materials*, vol. 44, no. 26, pp. 3133–3150, 2010, doi: 10.1177/0021998310371547.
- [47] R. C. Batra, G. Gopinath, and J. Q. Zheng, Material parameters for pressure-dependent yielding of unidirectional fiber-reinforced polymeric composites, *Composites Part B: Engineering*, vol. 43, no. 6, pp. 2594–2604, 2012, doi: 10.1016/J.COMPOSITESB.2011.12.005.
- [48] M. Vogler, H. Koerber, P. Kuhn, R. Rolfes, and P. Camanho, Constitutive modeling and experimental characterization of the non-linear stress-strain behavior of unidirectional carbon-epoxy under high strain rates, in *20th International Conference on Composite Materials*, Copenhagen, Denmark, 2015.
- [49] P. H. Petit and M. E. Waddoups, A Method of Predicting the Nonlinear Behavior of Laminated Composites, *Journal of Composite Materials*, vol. 3, no. 1, pp. 2–19, 2016, doi: 10.1177/002199836900300101.
- [50] A. Matzenmiller, J. Lubliner, and R. L. Taylor, A constitutive model for anisotropic damage in fiber-composites, *Mechanics of Materials*, vol. 20, no. 2, pp. 125–152, 1995, doi: 10.1016/0167-6636(94)00053-0.
- [51] Y. Chen, Y. Zhao, S. Ai, C. He, Y. Tao, Y. Yang, and D. Fang, A constitutive model for elastoplastic-damage coupling effect of unidirectional fiber-reinforced polymer matrix composites, *Composites Part A: Applied Science and Manufacturing*, vol. 130, 2020, doi: 10.1016/J.COMPOSITESA.2019.105736.
- [52] D. Vasiukov, S. Panier, and A. Hachemi, Non-linear material modeling of fiber-reinforced polymers based on coupled viscoelasticity–viscoplasticity with anisotropic continuous damage mechanics, *Composite Structures*, vol. 132, pp. 527–535, 2015, doi: 10.1016/J.COMPSTRUCT.2015.05.027.
- [53] Y. Wang, D. Chen, N. Li, H. Yuan, Z. Zhu, Y. Li, and Z. Huang, A micromechanics based elasto-plastic damage model for unidirectional composites under off-axis tensile loads, *Scientific Reports*, vol. 10, no. 1, 2020, doi: 10.1038/s41598-020-57771-8.
- [54] C. Schuecker and H. E. Pettermann, Combining Elastic Brittle Damage with Plasticity to Model the Non-linear behavior of Fiber Reinforced Laminates, *Computational Methods in Applied Sciences*, vol. 10, pp. 99–117, 2008, doi: 10.1007/978-1-4020-8584-0\_5.
- [55] T. Wehrkamp-Richter, R. Hinterhölzl, and S. T. Pinho, Damage and failure of triaxial braided composites under multi-axial stress states, *Composites Science and Technology*, vol. 150, pp. 32–44, 2017, doi: 10.1016/J.COMPSCITECH.2017.07.002.
- [56] P. Ladeveze and E. LeDantec, Damage modelling of the elementary ply for laminated composites, *Composites Science and Technology*, vol. 43, no. 3, pp. 257–267, 1992, doi: 10.1016/0266-3538(92)90097-M.
- [57] J. Fitoussi, F. Meraghni, Z. Jendli, G. Hug, and D. Baptiste, Experimental methodology for high strain-rates tensile behaviour analysis of polymer matrix composites, *Composites Science and Technology*, vol. 65, no. 14, pp. 2174–2188, 2005, doi: 10.1016/J.COMPSCITECH.2005.05.001.

- [58] G. Hug, Behaviour analysis of carbon-epoxy laminates under high-speed loading: manufacture of the same materials by means of microwave curing for comparison, Arts et Métiers ParisTech, Paris, 2005.
- [59] M. Castres, Modélisation dynamique avancée des composites à matrice organique (CMO) pour l'étude de la vulnérabilité des structures aéronautiques, Ecole Centrale de Lille, 2018.
- [60] Z. Zhai, B. Jiang, and D. Drummer, Characterization of nonlinear response in quasi-unidirectional E-glass fabric reinforced polypropylene composites under off-axis tensile loading, *Polymer Testing*, vol. 63, pp. 521–529, 2017, doi: 10.1016/J.POLYMERTESTING.2017.09.019.
- [61] J. Xie, G. Fang, Z. Chen, and J. Liang, Modeling of Nonlinear Mechanical Behavior for 3D Needled C/C-SiC Composites Under Tensile Load, *Applied Composite Materials*, vol. 23, no. 4, pp. 783–797, 2016, doi: 10.1007/S10443-016-9485-4.
- [62] S. N. A. Safri, M. T. H. Sultan, N. Yidris, and F. Mustapha, Low Velocity and High Velocity Impact Test on Composite Materials-A review 1, *The International Journal Of Engineering And Science (IJES)*, vol. 3, no. 9, pp. 50–60, 2014.
- [63] W. J. Cantwell and J. Morton, The influence of varying projectile mass on the impact response of CFRP, *Composite Structures*, vol. 13, no. 2, pp. 101–114, 1989, doi: 10.1016/0263-8223(89)90048-2.
- [64] M. Chandrasekar, M. R. Ishak, M. Jawaid, S. M. Sapuan, and Z. Leman, Low velocity impact properties of natural fiber-reinforced composite materials for aeronautical applications, in *Sustainable Composites for Aerospace Applications*, Elsevier, 2018, pp. 293–313. doi: 10.1016/B978-0-08-102131-6.00014-1.
- [65] H. M. Hsiao and I. M. Daniel, Strain rate behavior of composite materials, *Composites Part B: Engineering*, vol. 29, no. 5, pp. 521–533, 1998, doi: 10.1016/S1359-8368(98)00008-0.
- [66] W. J. Cantwell and J. Morton, The impact resistance of composite materials — a review, *Composites*, vol. 22, no. 5, pp. 347–362, 1991, doi: 10.1016/0010-4361(91)90549-V.
- [67] R. Ecault, M. Boustie, F. Touchard, F. Pons, L. Berthe, L. Chocinski-Arnault, B. Ehrhart, and C. Bockenheimer, A study of composite material damage induced by laser shock waves, *Composites Part A: Applied Science and Manufacturing*, vol. 53, pp. 54–64, 2013, doi: 10.1016/J.COMPOSITESA.2013.05.015.
- [68] M. Perton, A. Blouin, and J.-P. Monchalain, Adhesive bond testing of carbon-epoxy composites by laser shockwave, *Journal of Physics D: Applied Physics*, vol. 44, no. 3, p. 34012, 2011, doi: 10.1088/0022-3727/44/3/034012.
- [69] R. Ecault, Etude expérimentale et numérique du comportement dynamique de composites aéronautiques sous choc laser . Optimisation du test d'adhérence par ondes de choc sur les assemblages composites collées, Ecole Nationale Supérieure de Mécanique et d'Aérotechnique - Poitiers, 2013.
- [70] E. Gay, L. Berthe, M. Boustie, M. Arrigoni, and M. Trombini, Study of the response of CFRP composite laminates to a laser-induced shock, *Composites Part B: Engineering*, vol. 64, pp. 108–115, 2014, doi: 10.1016/j.compositesb.2014.04.004.
- [71] M. Ghrib, L. Berthe, N. Mechbal, M. Rébillat, M. Guskov, R. Ecault, and N. Bedreddine, Generation of controlled delaminations in composites using symmetrical laser shock configuration, *Composite Structures*, vol. 171, pp. 286–297, 2017, doi: 10.1016/j.compstruct.2017.03.039.
- [72] J. Harding and L. M. Welsh, A tensile testing technique for fibre-reinforced composites at impact rates of strain, *Journal of Materials Science*, vol. 18, no. 6, pp. 1810–1826, 1983,

doi: 10.1007/BF00542078.

- [73] J. Kwon, J. Choi, H. Huh, and J. Lee, Evaluation of the effect of the strain rate on the tensile properties of carbon–epoxy composite laminates, *Journal of Composite Materials*, vol. 51, no. 22, pp. 3197–3210, 2017, doi: 10.1177/0021998316683439.
- [74] A. Gilat, R. K. Goldberg, and G. D. Roberts, Experimental study of strain-rate-dependent behavior of carbon/epoxy composite, *Composites Science and Technology*, vol. 62, no. 10–11, pp. 1469–1476, 2002, doi: 10.1016/S0266-3538(02)00100-8.
- [75] R. M. White, Generation of elastic waves by transient surface heating, *Journal of Applied Physics*, vol. 34, no. 12, pp. 3559–3567, 1963, doi: 10.1063/1.1729258.
- [76] J. P. Romain and D. Zagouri, Laser-shock studies using an electromagnetic gauge for particle measurements, in *Shock Compression of Condensed Matter–1991*, Elsevier, 1992, pp. 801–804. doi: 10.1016/b978-0-444-89732-9.50183-7.
- [77] L. Tollier, E. Bartnicki, and R. Fabbro, Experimental and numerical study of laser-driven spallation with visar diagnostic, in *AIP Conference Proceedings*, AIP Publishing, 1996, pp. 1265–1268. doi: 10.1063/1.50867.
- [78] F. Cottet and M. Boustie, Spallation studies in aluminum targets using shock waves induced by laser irradiation at various pulse durations, *Journal of Applied Physics*, vol. 66, no. 9, pp. 4067–4073, 1989, doi: 10.1063/1.343991.
- [79] M. Boustie, F. Cottet, and J. P. Romain, Spalling due to a strong shock wave decay process in solid targets irradiated by a pulsed laser, in *Shock Compression of Condensed Matter–1991*, Elsevier, 1992, pp. 805–808. doi: 10.1016/b978-0-444-89732-9.50184-9.
- [80] J. Yuan and V. Gupta, Measurement of interface strength by the modified laser spallation technique. I. Experiment and simulation of the spallation process, *Journal of Applied Physics*, vol. 74, no. 4, pp. 2388–2396, 1993, doi: 10.1063/1.354698.
- [81] J. C. J. Duke, E. G. I. Henneke, and W. W. Stinchcomb, Ultrasonic stress wave characterization of composite materials - NASA-CR-3976, Cleveland, Ohio, 1986.
- [82] I. A. . Novikov S.A., Divnov I.I., The Study of Fracture of Steel, Aluminum, and Copper under Explosive Loading, *Physics of Metals and Metallography*, vol. 21(4), pp. 608–6015, 1966.
- [83] L. M. Barker and R. E. Hollenbach, Laser interferometer for measuring high velocities of any reflecting surface, *Journal of Applied Physics*, vol. 43, no. 11, pp. 4669–4675, 1972, doi: 10.1063/1.1660986.
- [84] P. D. Sargis, N. E. Molau, D. Sweider, M. E. Lowry, and O. T. Strand, Photonic Doppler Velocimetry, 1999.
- [85] E. Gay, Comportement de composites sous choc induit par laser : développement de l’essai d’adhérence par choc des assemblages de composites collés, ’École Nationale Supérieure d’Arts et Métiers Paris, 2011.
- [86] M. Scius-Bertrand, Endommagements maîtrisés par chocs laser symétriques et désassemblages des collages, HESAM Université, 2021.
- [87] R. Amacher, J. Cugnoni, J. Botsis, L. Sorensen, W. Smith, and C. Dransfeld, Thin ply composites: experimental characterization and modeling of size-effects, *Composites Science and Technology*, vol. 101, pp. 121–132, 2014, doi: 10.1016/j.compscitech.2014.06.027.
- [88] V. M. Cuartas, M. Perrin, M.-L. Pastor, H. Welemane, A. Cantarel, M. Karama, and V. Munoz, Determination of the elastic properties in CFRP composites: comparison of different approaches based on tensile tests and ultrasonic characterization, *Advances in*

- Aircraft and Spacecraft Science*, vol. 2, no. 3, pp. 249–260, 2014, doi: 10.12989/aas.2015.2.3.249i.
- [89] J. Bora and S. Kirtania, Comparative study of elastic properties and mode I fracture energy of carbon nanotube/epoxy and carbon fibre/epoxy laminated composites, *Micro and Nano Systems Letters*, vol. 8, no. 1, pp. 1–10, 2020, doi: 10.1186/S40486-020-00120-1.
- [90] C. Venkateshwar Reddy, C. Joseph S Raju, P. Ramesh Babu, and R. Ramnarayan, Mechanical Characterization of Carbon/Epoxy Unidirectional and Bidirectional Composites for Structural Application, *Journal of Engineering Research and Application*, vol. 8, no. 7–III, pp. 21–24, 2018, doi: 10.9790/9622-080703212421|P.
- [91] G. A. Bibo, P. J. Hogg, and M. Kempb, Mechanical Characterisation Of Glass-and Carbon-Fibre-Reinforced Composites Made With Non-Crimp Fabrics, *Composite Science and Technology*, vol. 57, no. 9–10, pp. 1221–1241, 1997, doi: 10.1016/S0266-3538(97)00053-5.
- [92] N. Tual, Durability of carbon / epoxy composites for tidal turbine blade applications, Université de Bretagne Occidentale, 2015.
- [93] G. Tahan, M. Arrigoni, P. Bidaud, L. Videau, and D. Thévenet, Evolution of failure pattern by laser induced shockwave within an adhesive bond, *Optics & Laser Technology*, vol. 129, p. 106224, 2020, doi: 10.1016/J.OPTLASTEC.2020.106224.
- [94] M. Ayad, S. Ünaldi, M. Scius-Bertrand, C. Le Bras, B. Fayolle, and L. Berthe, Dynamical modeling of bi-layer Aluminium adhesive tape for laser shock applications, *Optics & Laser Technology*, vol. 163, p. 109366, 2023, doi: 10.1016/J.OPTLASTEC.2023.109366.
- [95] L. Berthe, R. Fabbro, P. Peyre, L. Tollier, and E. Bartnicki, Shock waves from a water-confined laser-generated plasma, *Journal of Applied Physics*, vol. 82, no. 6, pp. 2826–2832, 1997, doi: 10.1063/1.366113.
- [96] C. S. Alexander, C. T. Key, and S. C. Schumacher, Dynamic response and modeling of a carbon fiber - Epoxy composite subject to shock loading, *Journal of Applied Physics*, vol. 114, no. 22, p. 223515, 2013, doi: 10.1063/1.4846116.
- [97] J. A. Smith, J. M. Lacy, D. Lévesque, J. P. Monchalín, and M. Lord, Use of the Hugoniot elastic limit in laser shockwave experiments to relate velocity measurements, *AIP Conference Proceedings*, vol. 1706, no. 1, p. 47, 2016, doi: 10.1063/1.4940537/585873.